1988

Micromagnetic study of the double-layered MR elements

Hah Young Yoo
Iowa State University

Order Number 8825967

Micromagnetic study of the double-layered MR elements

Yoo, Hah Young, Ph.D.

Iowa State University, 1988

U·M·I
300 N. Zeeb Rd.
Ann Arbor, MI 48106

PLEASE NOTE:

In all cases this material has been filmed in the best possible way from the available copy. Problems encountered with this document have been identified here with a check mark ___√___.

1. Glossy photographs or pages _____
2. Colored illustrations, paper or print _____
3. Photographs with dark background _____
4. Illustrations are poor copy _____
5. Pages with black marks, not original copy _____
6. Print shows through as there is text on both sides of page _____
7. Indistinct, broken or small print on several pages ___✓___
8. Print exceeds margin requirements _____
9. Tightly bound copy with print lost in spine _____
10. Computer printout pages with indistinct print _____
11. Page(s) _____ lacking when material received, and not available from school or author.
12. Page(s) _____ seem to be missing in numbering only as text follows.
13. Two pages numbered _____. Text follows.
14. Curling and wrinkled pages _____
15. Dissertation contains pages with print at a slant, filmed as received _____
16. Other _____

_____

_____

Micromagnetic study of the double-layered MR elements

by

Hah Young Yoo

A Dissertation Submitted to the
Graduate Faculty in Partial Fulfillment of the
Requirements for the Degree of
DOCTOR OF PHILOSOPHY

Department: Electrical Engineering and Computer Engineering
Major: Computer Engineering

Approved:

Signature was redacted for privacy.

In Charge of Major Work

Signature was redacted for privacy.

For the Major Department

Signature was redacted for privacy.

For the Graduate College

Iowa State University
Ames, Iowa
1988

TABLE OF CONTENTS

LIST OF TABLES

LIST OF FIGURES

1. INTRODUCTION

1.1. Anisotropic Magnetoresistance

The anisotropic magnetoresistance(MR) effect found in 3-d transition metals and alloys is the outcome of the resistivity difference between the parallel resistivity ($\rho_{||}$) and the perpendicular resistivity ($\rho_{\perp}$) with respect to the direction of internal magnetization $\vec{M}$. The difference $\Delta\rho = \rho_{||} - \rho_{\perp}$ is called the anisotropic resistivity and the MR ratio is defined as $\Delta\rho/\rho_{av}$, where $\rho_{av} = (\rho_{||} + 2\rho_{\perp})/3$ [1]. The MR ratio varies depending upon the manufacturing process, dimension of the device, and the annealing process, as well as the material. A typical value of the MR ratio is 2-3% for the non-magnetostrictive permalloy($Ni_{80}Fe_{20}$).

The origin of this effect is the quantum mechanical interaction of the charge carriers and is beyond the scope of this dissertation. To understand this effect phenomenologically the magnetic thin film element in which the electric field E is applied in the x-direction and the magnetic field H is applied in the y-direction is drawn in Figure 1.1a. The electric field induces the x-directional current density J and the magnetic field rotates $\vec{M}$ such that it makes angle θ with x-direction. The electric field and the current density can be decomposed into the parallel and perpendicular components with respect to $\vec{M}$ as shown in Figure 1.1b. Then, we

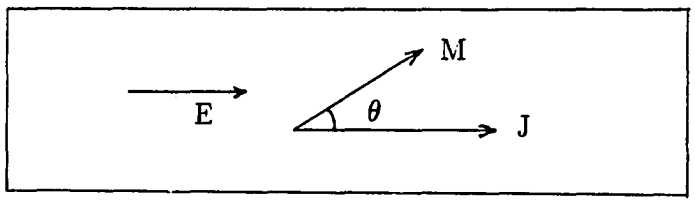

(a)

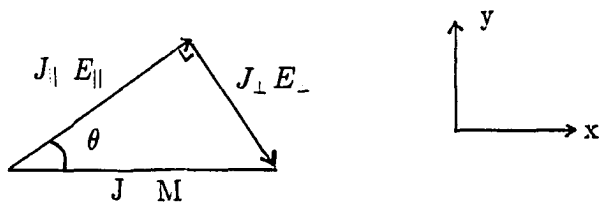

(b)

Figure 1.1: Thin MR element

can express E as follows [2].

$$E = E_{\|}\cos\theta + E_{\perp}\sin\theta \tag{1.1}$$

Since the resistivity is defined as $\rho = E/J$, Equation (1.1) can be written as

$$\begin{aligned} E &= \rho_{\|}J_{\|}\cos\theta + \rho_{\perp}J_{\perp}\sin\theta \\ &= \rho_{\|}J\cos^2\theta + \rho_{\perp}J\sin^2\theta \\ &= J\left((\rho_{\perp} + \Delta\rho)\cos^2\theta + \rho_{\perp}\sin^2\theta\right) \\ &= J\left(\rho_{\perp} + \Delta\rho\cos^2\theta\right). \end{aligned} \tag{1.2}$$

By combining Equation (1.2) and $\rho = E/J$ we have Equation (1.3) which is commonly used to describe the anisotropic MR effect.

$$\rho = \rho_{\perp} + \Delta\rho\cos^2\theta \tag{1.3}$$

Since the direction of $\vec{M}$ in the ferromagnetic thin film can be changed easily by a small external field, the MR effect described in Equation (1.3) can be used for the detection of the states in the magnetic memory systems.

1.2. MR Effect for Magnetic Sensor

The first successful application of the MR effect was made by Hunt [3] when he proposed a magnetic read head based on MR effect in 1971. Since then continued interest [4]-[9] has existed in using the MR effect as the magnetic sensor because of the following advantages [10] of the MR sensor over the conventional inductive read head. First, the anisotropy resistivity ($\Delta\rho$) in a MR sensor is a fixed quantity under ordinary operating condition. Therefore, the output can be made larger by increasing the applied current which is only limited by thermal effects. Second, since well advanced thin film photolithographic techniques are used for the fabrication of the MR sensors, the multitrack MR sensor designed for high density recording environments is fabricated more easily than the comparably complex inductive sensor. Finally, the sensor outputs are independent of relative speed between sensor and medium since it detects the magnetic flux itself rather than the change of flux. This feature is especially useful for low speed recording environments.

However, the reduction of noise and the linearization of the sensor response are considered to be the most important issues affecting wide commercialization of MR sensors. The noise in the MR sensors, so called Barkhausen noise, is closely related to the abrupt motion of domain walls in the device. The reduction of the size of the device has been suggested as the possible solution to the noise problem. It was believed that the small geometry of the device would lead to a single domain state

since the exchange energy which tends to keep the magnetization in one direction dominates the other energies in such a device. However, Kryder et al. [11] reported that the the dimension appropriate for the MR sensor is not small enough to generate the single domain state. Instead, they found buckling domains at the edge of the device. These buckling domains, believed to be the source of the noise in the small MR sensor, are formed mainly because of the demagnetizing field at the edge of the device. The reduction of the demagnetizing field is therefore expected to lead to better noise performance in the MR sensor. The following are the means used to reduce the demagnetizing field in the MR sensors. First, the demagnetizing field effect at the center of the device can be reduced by increasing the length of the device. Since only the central part of the MR sensor is actively used for sensing, this method can be quite effective when the track width of the medium is large enough to allow a long sensor. A second method uses the magnetostatic coupling. Ooyen et al.[12] reported that sandwich structured films in which two homogeneous magnetic layers are separated by a nonmagnetic layer can produce a large reduction in magnetostatic energy(demagnetizing field). It was further reported by Berchier et al. [13] that this structure indeed leads to a significant reduction in the domain walls, exhibiting a better noise performance in the devices.

As shown in Equation (1.3) the MR response is proportional to $\cos^2\theta$. Therefore, the sensitivity which can be defined as $-d\rho/d\theta$ is proportional to $\sin 2\theta$ and attains its maximum value when the magnetization $\vec{M}$ is biased to make an angle of 45° with the applied current. It can be also shown that the maximum linear response is obtained at the same bias. Therefore, the various biasing schemes have been investigated to achieve the maximum sensitivity and linearity. The most com-

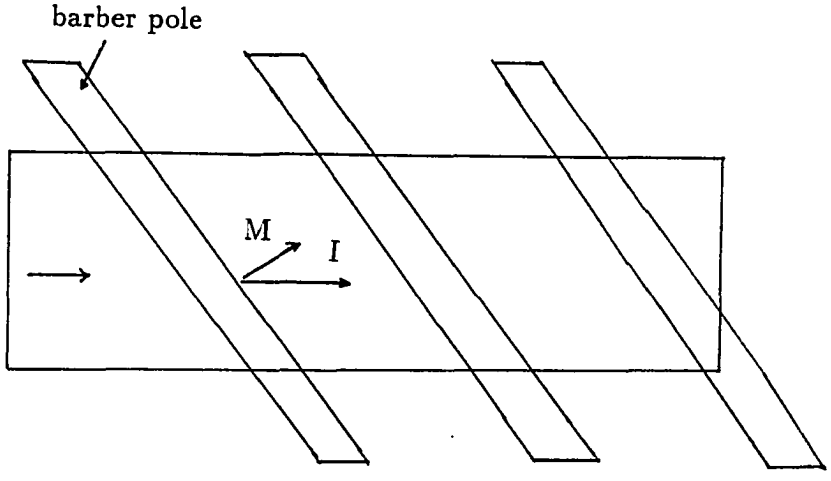

Figure 1.2: Barber pole biasing scheme

monly used biasing scheme at present is the barber pole biasing in which highly conductive metal bars are inserted into the MR device [14]. These conducting bars are slanted as shown in Figure 1.2 to divert the direction of current locally from the average current direction. The reduced response and the nonuniform distribution of current density as well as the complexity of the structure are cited as the problems of this scheme.

Another biasing scheme uses a multilayer structure. First, the MR sensor which is made from soft magnetic material can be biased by the hard magnetic material attached to it. In this scheme the critical issue is the choice of a good hard magnetic material. Currently, no material is known to be the best. A second method of multilayer biasing comes from the sandwich structure device described earlier. In the sandwich structure, the current in one layer produces the magnetic field which rotates the magnetization in the other magnetic layer. The current therefore is used

for the biasing purpose as well as for the sensing purpose.

The discussions so far have emphasized that the sandwich structured device can provide both the reduction of noise and the linearization of response, the two most important requirements for successful MR sensors. Therefore, it can be concluded that the sandwich structure is very promising structure for MR sensors.

1.3. MR Effect Used in Memory Elements

The first attempt to use the MR effect for the detection of a magnetic memory element by directly flowing the sense current in the memory element itself was made by Schwee et al. [15]. They proposed a crosstie memory in which 1-state is represented by the presence of Bloch line pair while 0-state is represented by the absence of the Bloch line in the crosstie wall. It is well known that the crosstie wall occurs at the thickness around 300-600 $\AA$ as an intermediate state between the Bloch wall and Néel wall [16]. However, a reliable analytic model is not available to predict and optimize the performance of this type of memory. Therefore, a trial and error method was developed to discover the geometries which support the stable operations of the creation, annihilation and propagation of the Bloch lines in the crosstie wall. As a result, special structures such as serrated stripes [17] and snake shaped geometry [18] were suggested. It is not likely that this approach will lead to a successful commercial memory system because of the small output signal level and the lack of proper analysis model. This work, however, opened the possibility of developing MR memory element which has the following advantages. First, a MR memory system could be produced by a planar photolithographic procedure. Thus, it could be fabricated along with the semiconductor devices such as drivers,

decoders, and sense amplifiers in the same chip. Second, since it is magnetic, it is radiation hard and nonvolatile. Finally, low cost, low power consumption and high density can be achieved.

Encouraged by the potential advantages of the MR memory system listed above, A. V. Pohm and Honeywell Inc. launched a project to develop a memory system based on the MR effect. The rectangular geometry similar to the magnetic sensor was proposed as a basic element. In the memory system the domain walls are even more detrimental than in the sensor since they are responsible for inconsistent switching behavior as well as for the noise problem. Thus the sandwich structure which is capable of reducing the magnetostatic energy seems to be very an attractive choice for the memory element too.

To optimize the design parameters and to predict the behavior of the sandwich structured elements it is necessary to have a proper analysis tool. This dissertation describe the development an analysis tool based on the micromagnetic equation. 1-dimensional models based on micromagnetic equation for this structure have appeared previously [19]-[20]. In this dissertation, a 2-dimensional analysis model will be presented under the appropriate assumptions.

2. MICROMAGNETIC EQUATIONS

2.1. Introduction

Generally, magnetic problems are treated in four different levels depending on the dimensions of the specimen of interest and the degree of approximation involved. These four levels are the macroscopic level, the domain level, the microscopic level, and the atomic level [21].

The atomic level treatment, which actually concerns the interactions of the individual atoms, requires the quantum mechanical treatment. Thus, this treatment is probably beyond engineering interest and will not be discussed further.

At the macroscopic level the linearizable behaviors of magnetic material are described by constant parameters such as permeability or susceptibility while non-linear and anisotropic behaviors are described by M-H loops and the permeability tensor. A magnetic circuit analog to a lumped electric circuit model is a typical example of the macroscopic level treatment.

At the domain level [22], two distinctive regions, domains and domain walls, are assumed to exist as independent entities. Here the domain is defined as the region in which the magnetization is saturated in one direction, and the domain walls are regarded as the transition regions of magnetization between domains. At this level, the direction of the magnetization in the domains and the positions of

the walls are two independent variables which can be determined by minimizing the total free energy of the system. However, a energy minimum state obtained by this method is only a relative energy minimum state, since it is determined by comparison with the other reasonable energy states. Thus, the solution depends somewhat on the ingenuity of the researcher and can not always be confirmed as the true minimum state.

The micromagnetic treatment [23] starts by eliminating the distinction between the domain and the domain walls. According to this approach the domain walls, if they exist, should show up from the minimization of the total energy as the regions in which the magnetization changes very rapidly compared to the magnetization changes of the remaining regions, which can be thought as the domains. Here, the magnitude of the magnetization M is assumed to be constant and the independent variable is the direction of the magnetization which is allowed to vary continuously in position. It is well known that the magnitude of magnetization is only a function of the temperature. Thus, the above assumption is justified when the temperature change can be ignored.

The basic principles of micromagnetics were first formulated by Landau and Lifschitz [24], and were further developed by Brown. In the micromagnetic calculations the stable equilibrium state is obtained by minimizing the total free energy which is given as the function of the magnetization direction. The total energy of the system consists of the exchange energy, the anisotropy energy, the demagnetizing energy and the external energy. In the following sections the discussions on the origin and the role of the each energy term will be followed by the derivation of its mathematical expression. In the last section of this chapter, the micromag-

netic equation will be derived by applying the variational technique on the total free energy of the system.

2.2. Exchange Energy

Ferromagnetic materials are characterized by spontaneous magnetization. This characteristic was first explained by Weiss' molecular field which was replaced by the exchange force of Heisenberg. The origin of the exchange force is the quantum mechanical coupling of the angular momentum of the atoms. Two different mechanisms are responsible for the angular momentum. One is the spin angular momentum coming from the spin motion of the electrons and the other is the orbital angular momentum associated with the orbital motion of electrons around nucleus [25]. The uncompensated spin angular momentum is especially responsible for the ferromagnetic property of 3-d transition metals, i.e., Ni, Fe and Co.

To express the exchange energy of the continuous medium in a manageable mathematical form we start by considering the exchange energy of the two neighboring electron spins as shown in Equation (2.1).

$$W_{ij} = -2J\vec{S}_i \cdot \vec{S}_j \tag{2.1}$$

where J is a constant and $\vec{S}_i\hbar$ is the spin angular momentum of spin i. Under the assumption that the angle difference between spins i and j is very small we have,

$$\begin{aligned} \vec{S}_i \cdot \vec{S}_j &= S^2 \cos\theta_{ij} \\ &\cong S^2\left(1 - 0.5{\theta_{ij}}^2\right) \\ &= S^2\left(1 - 0.5\left(\vec{m}_j - \vec{m}_j\right)^2\right) \end{aligned} \tag{2.2}$$

where $S = \left|\vec{S}_i\right| = \left|\vec{S}_j\right|$ and θ_{ij} is the angle difference between spins i and j and $\vec{m}_i$ is the directional unit vector of S_i.

The directional unit vector $\vec{m}$ of the continuous magnetization $\vec{M}$ can be defined as Equation (2.3) in the cartesian coordinate system.

$$\vec{m} = \alpha\vec{x} + \beta\vec{y} + \gamma\vec{z} \tag{2.3}$$

where α, β and γ are the directional cosines and $\vec{x}$, $\vec{y}$ and $\vec{z}$ designate the unit vectors of the cartesian coordinates x, y and z respectively. If we assume that the discrete unit vector $\vec{m}_i$ can be approximated by the continuous unit vector $\vec{m}$, then we have,

$$\vec{m}_j - \vec{m}_i = \vec{s}_j \cdot \nabla\vec{m} \tag{2.4}$$

where $\vec{s}_j$ is the position vector of spin j. By substituting Equations (2.2) and (2.4) into Equation (2.1) we get Equation (2.5).

$$W_{ij} = -2J^2S^2\left(1 - 0.5\left(\vec{s}_j \cdot \vec{m}\right)^2\right) \tag{2.5}$$

We are not interested in the constant part in Equation (2.5) since the application of the variational method will eliminate the constant terms. Thus, we can rewrite Equation (2.5) as Equation (2.6).

$$w_{ij} = JS^2\left(\vec{s}_j \cdot \nabla\vec{m}\right)^2 \tag{2.6}$$

Under the assumption that n is the number of spins per unit volume the exchange energy density becomes

$$w_e = 0.5nJS^2\sum_j\left(\vec{s}_j \cdot \nabla\vec{m}\right)^2. \tag{2.7}$$

For a cubic crystal Equation (2.7) becomes,

$$w_e = A\left((\nabla\alpha)^2 + (\nabla\beta)^2 + (\nabla\gamma)^2\right) \tag{2.8}$$

where

$$A = \frac{1}{6}nJS^2\sum_j {s_j}^2 = \frac{JS^2c}{a}.$$

and where a is the length of the unit cell and $c = 1, 2$ and 4 for simple, body-centered and face-centered cubic, respectively. Since the major portions of the material of interest are cubic structured, Equation (2.8) will be used as the exchange energy density term for future discussion.

2.3. Demagnetizing Energy

The demagnetizing field can be found in all the magnetic material since the source of the magnetization in the material is the magnetic dipole. Thus, the bar magnet shown in Figure 2.1 has the inseparable N pole and S pole regardless of its dimension. The magnetic field starting from the N pole terminates on the S pole as shown in the Figure 2.1. Inside the bar magnet the magnetization $\vec{M}$, which is the source of the magnetic field, is in the opposite direction to the magnetic field. As a result the magnetic poles, generated mainly by the discontinuity of the magnetization $\vec{M}$ at the surface, tend to be weakened by the opposing field they generate. This internal field is called the demagnetizing field since it tends to demagnetize the bar magnet. This phenomenon can be explained in a different perspective with the aid of Maxwell's equations. From Maxwell's equations, we know that $\nabla \cdot \vec{B} = 0$. By combining this with the relation $\vec{B} = \vec{H} + 4\pi\vec{M}$, in cgs units, we have $\nabla \cdot \vec{H} = -4\pi\nabla \cdot \vec{M}$. This relation clearly shows that if there is a

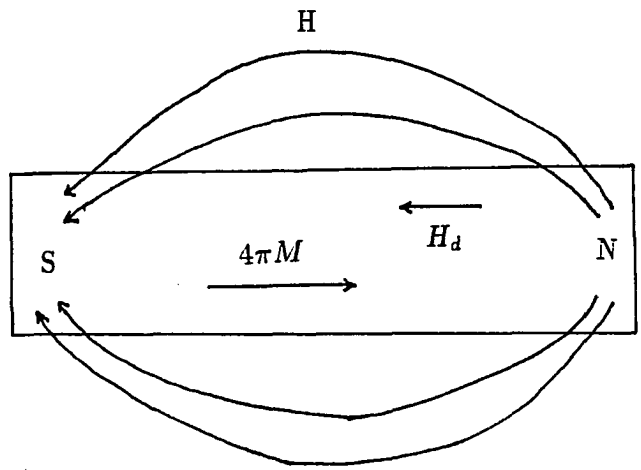

Figure 2.1: Demagnetizing field in bar magnet

magnetic pole which is $4\pi\nabla\cdot\vec{M}$, then there is a field which opposes it. Again this is the demagnetizing field. Thus, the demagnetizing field can be calculated from the knowledge of the magnetization distribution in the material. To be more specific, the demagnetizing field arises from the free magnetic poles created by $\nabla\cdot\vec{M}$ inside the material and by $\vec{n}\cdot\vec{M}$ at the surface. Thus, we can define the scalar potential Φ from which the demagnetizing field can be calculated by Equation (2.9).

$$H_d = -\nabla\Phi \tag{2.9}$$

Here, Φ should satisfy the following equations.

$$\nabla^2\Phi = 4\pi\nabla\cdot\vec{M}, \quad \textit{inside} \tag{2.10}$$

$$\nabla^2\Phi = 0, \quad \textit{outside} \tag{2.11}$$

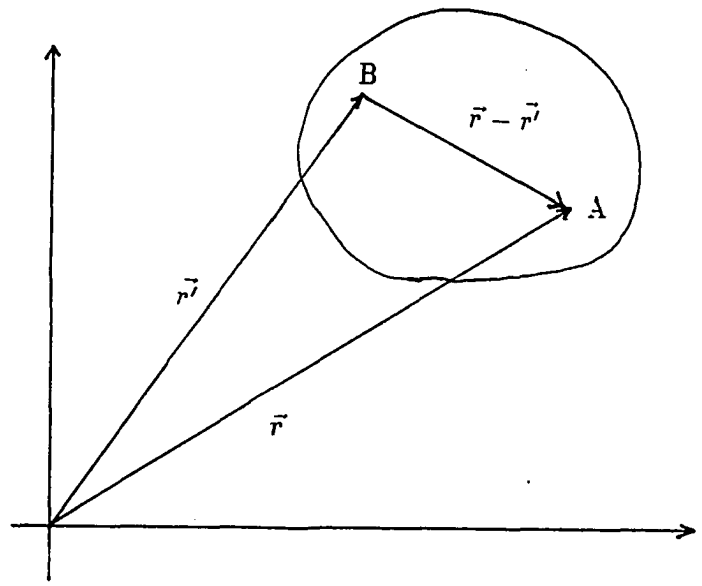

Figure 2.2: Calculation of magnetic potential

and at the surface,

$$-\frac{\partial\Phi\left(0^{+}\right)}{\partial n}+4\pi\vec{n}\cdot\vec{M}\left(0^{+}\right)=-\frac{\partial\Phi\left(0^{-}\right)}{\partial n} \tag{2.12}$$

$$\Phi\left(0^{+}\right)=\Phi\left(0^{-}\right) \tag{2.13}$$

or by the direct integration of volume and surface poles, we have,

$$\Phi\left(\vec{r}\right)=\int\frac{-\nabla'\cdot\vec{M}\left(\vec{r'}\right)}{\mid\vec{r}-\vec{r'}\mid}dv'+\int\frac{\vec{n'}\cdot\vec{M}\left(\vec{r'}\right)}{\mid\vec{r}-\vec{r'}\mid}dS' \tag{2.14}$$

where $\vec{n}$ and $\vec{n'}$ are unit vectors outwardly normal to the surface and $\vec{r}$ and $\vec{r'}$ are position vectors as shown in Figure 2.2. Equation (2.14) represents the potential of point B due to all the magnetic poles in the material as shown in Figure 2.2. Then, the demagnetizing energy density can be expressed as Equation (2.15).

$$w_d=-0.5\vec{H}_d\cdot\vec{M} \tag{2.15}$$

The factor 0.5 in Equation (2.15) results from the fact that the demagnetizing field arises directly from the internal magnetization $\vec{M}$ itself.

2.4. Anisotropy Energy

It is well known that the polycrystalline thin film produced under the influence of the strong field has uniaxial anisotropy. Since MR devices are made of such polycrystalline thin films the discussion will be centered on the uniaxial anisotropy. In the uniaxially anisotropic films, the axis along which the magnetization prefers to lie is defined as the easy axis and the axis perpendicular to the easy axis is called the hard axis. Phenomenologically, this energy density is described by Equation (2.16).

$$w_a = K\sin^2\theta \tag{2.16}$$

where

$$K = \frac{H_k M_s}{2}$$

and θ is the angle between the magnetization and the easy axis. H_k is called the uniaxial anisotropy constant and M_s is the saturation magnetization.

Another anisotropy energy comes from the surface effect of the magnetic material. The incomplete distribution of dipoles at the surface influences the magnetostatic energy and the exchange energy as well as the anisotropic energy [26]. This effect is summarized by Equation (2.17) phenomenologically.

$$w_s = 0.5K_s(\vec{n}\cdot\vec{m})^2 \tag{2.17}$$

where $\vec{n}$ is the unit vector which is outwardly orthogonal to the surface and K_s is the surface anisotropy constant.

2.5. Micromagnetic Equation

The total free energy of the system is obtained by summing up all the energy terms discussed so far along with the external energy which comes from the external magnetic field source. Thus, total free energy of the system becomes,

$$G = \int \left(A \left((\nabla\alpha)^2 + (\nabla\beta)^2 + (\nabla\gamma)^2 \right) + w_a - 0.5\vec{M} \cdot \vec{H}_d - \vec{M} \cdot \vec{H}_0 \right) dv + \int 0.5 K_s (\vec{n} \cdot \vec{m})^2 \, dS \quad (2.18)$$

where $\vec{H}_0$ is the external field.

The equilibrium condition is obtained by requiring $\partial G = 0$. Since the application of variation method on internal magnetization $\vec{M}$ results in Equation (2.19), it is obvious that ∂G will be given as a function of α, β and γ.

$$\partial\vec{M} = M_s \partial\vec{m} = M_s \partial (\alpha\vec{x} + \beta\vec{y} + \gamma\vec{z}) \quad (2.19)$$

To evaluate ∂G each term in Equation (2.18) should be examined. First, the process of variation on the exchange term can be described as follows:

$$\partial E_\alpha = \partial \int A (\nabla\alpha)^2 dv = 2A \int (\nabla\alpha \cdot \nabla\partial\alpha) dv \quad (2.20)$$

From the following relation,

$$\nabla \cdot (\nabla\alpha\partial\alpha) = \left(\nabla^2\alpha\right) \partial\alpha + \nabla\alpha \cdot \nabla\partial\alpha \quad (2.21)$$

Equation (2.20) becomes Equation (2.22).

$$\partial E_\alpha = 2A \int \nabla \cdot (\nabla\alpha\partial\alpha) dv - 2A \int \left(\nabla^2\alpha\right) \partial\alpha dv \quad (2.22)$$

Applying the divergence theorem to Equation (2.22), we have,

$$\partial E_\alpha = 2A \int \partial\alpha (\nabla\alpha) \cdot \vec{n} dS - 2A \int \left(\nabla^2\alpha\right) \partial\alpha dv \quad (2.23)$$

Since $\nabla\alpha \cdot \vec{n} = \partial\alpha/\partial n$ Equation (2.23) becomes Equation (2.24).

$$\partial E_\alpha = 2A \int \frac{\partial \alpha}{\partial n \partial \alpha} dS - 2A \int \left(\nabla^2 \alpha\right) \partial\alpha dv \tag{2.24}$$

By the same procedures, we can get similar expressions for ∂E_β and ∂E_γ. Then the variation on the exchange term can be expressed as

$$\partial E_{ex} = \partial E_\alpha + \partial E_\alpha + \partial E_\gamma =$$
$$2A \int \left(\frac{\partial \vec{m}}{\partial n}\right) \cdot \partial\vec{m} dS - 2A \int \left(\nabla^2 \vec{m}\right) \cdot \partial\vec{m} dv \tag{2.25}$$

where $\partial\vec{m} = \partial\alpha\vec{x} + \partial\beta\vec{y} + \partial\gamma\vec{z}$.

Next, let us consider the variation process applied to the demagnetizing energy term. That is,

$$-\partial \int \left(0.5\vec{M} \cdot \vec{H}_d\right) dv = -0.5 \int \left(\partial\vec{M} \cdot \vec{H}_d + \partial\vec{H}_d \cdot \vec{M}\right) dv \tag{2.26}$$

From the reciprocity theorem we can prove that $\vec{M} \cdot \partial\vec{H}_d = \vec{H}_d \cdot \partial\vec{M}$. Substituting this relation into the Equation (2.26), we get the Equation (2.27).

$$\partial E_d = -\int M_s \vec{H}_d \cdot \partial\vec{m} \tag{2.27}$$

The variation on the volume and the surface anisotropy energy terms are straightforward and the results ar

$$\int \frac{\partial E_a}{\partial\vec{m} \cdot \partial\vec{m}} dv$$

and

$$\int K_s (\vec{n} \cdot \vec{m})\, \vec{n} \cdot \partial\vec{m} dS,$$

respectively. The variation on the external energy term results in

$$\int M_s \vec{E}_0 \cdot \partial\vec{m} dv$$

where

$$\frac{\partial}{\partial \vec{m}} = \frac{\partial}{\partial \alpha}\vec{x} + \frac{\partial}{\partial \beta}\vec{y} + \frac{\partial}{\partial \gamma}\vec{z}$$

By collecting the terms discussed so far, we can get the variation of free energy ∂G as Equation (2.28).

$$\partial G = \int \left(-2A\nabla^2\vec{m} - M_s\vec{H}_d - M_s\vec{H}_0 + \frac{\partial E_a}{\partial \vec{m}}\right) \cdot \partial\vec{m}dv + \int \left(2A\frac{\partial \vec{m}}{\partial n} + K_s(\vec{n}\cdot\vec{m})\vec{n}\right) \cdot \partial\vec{m}dS \tag{2.28}$$

Since $\vec{m}\cdot\vec{m} = 1$, the application of variation on $\vec{m}\cdot\vec{m}$ will result in $\partial\vec{m}\cdot\vec{m} = 0$. Thus, $\partial\vec{m}$ and $\vec{m}$ are mutually orthogonal and $\partial\vec{m}$ can be expressed as Equation (2.29).

$$\partial\vec{m} = \partial\vec{\theta} \times \vec{m} \tag{2.29}$$

Where $\partial\vec{\theta}$ represents the variation of arbitrary angle. By substituting $\partial\vec{m}$ of Equation (2.29) into Equation (2.28) we get Equation (2.30).

$$\partial G = -\int \vec{m} \times \left(2A\nabla^2\vec{m} + M_s\vec{H}_d + M_s\vec{H}_0 - \frac{\partial E_a}{\partial \vec{m}}\right) \cdot \partial\vec{\theta}dv + \int \vec{m} \times \left(2A\frac{\partial \vec{m}}{\partial n} + K_s(\vec{n}\cdot\vec{m})\vec{n}\right) \cdot \partial\vec{\theta}dS \tag{2.30}$$

Since the condition $\partial G = 0$ should be satisfied for any $\partial\vec{\theta}$, we can deduce Equations (2.31) and (2.32) from Equation (2.30).

$$inside \quad \vec{m} \times \left(2A\nabla^2\vec{m} + M_s\vec{H}_d + M_s\vec{H}_0 - \frac{\partial E_a}{\partial \vec{m}}\right) = 0 \tag{2.31}$$

$$at\ surface \quad \vec{m} \times \left(2A\frac{\partial \vec{m}}{\partial n} + K_s(\vec{n}\cdot\vec{m})\vec{n}\right) = 0 \tag{2.32}$$

Equation (2.31) is known as the micromagnetic equation and Equation (2.32) provides the boundary condition to this equation. Although these equations represent three scalar equations, only two of them are mutually independent. Also these

equations have only two independent variables since we have the other condition, $\vec{m} \cdot \vec{m} = 1$. Equations (2.31) and (2.32) along with the equation used to calculate the demagnetizing field completely specify the equilibrium condition of a magnetic system. The stability of the solutions of the micromagnetic equation should be checked by the condition $\delta^2 G \geq 0$. However, the calculation of $\delta^2 G$ is extremely complex and even impossible in many cases. Thus, the stability of the solution is usually checked only empirically.

It is a mathematical fact that a boundary value problem can have either no solution or many solutions depending on the boundary values. This implies that the micromagnetic equation will have many solutions if this equation is a successful modelling of the magnetic systems. It has been proved that this equation does have many solutions, some of which actually confirm the experimental results. The possibility of many solutions also suggests that the actual state depends on the history of the magnetic systems as well as the given conditions.

Since the micromagnetic equation is highly nonlinear, very few analytic solutions are known so far. The nucleation field calculation of the infinite cylinder bar and the prediction of the magnetic state of the ellipsoid are probably the only examples of the analytic solutions of this equation [27]. In both cases special geometry of the problem made the simplification of the micromagnetic equation possible. In the case of the ellipsoid the exchange term is dropped out since all the magnetization is aligned in one direction. Also it was proved that the uniformly magnetized ellipsoid has a homogeneous demagnetizing field. Thus, only the anisotropy energy and the external energy terms are given as functions of position.

Generally, the solution of the micromagnetic equation is obtained by using a

numerical technique. Still not many numerical solutions are known due to the excessive computation time requirement and lack of an effective numerical technique. The one-dimensional treatment of the Bloch wall by Brown and Labonte [28] and the two dimensional solution of the Bloch wall by Labonte [29] are the classical examples of the numerical solutions of the micromagnetic equation. Recently, one-dimensional solutions on the double layered thin film device have been reported by various authors [19]-[20] and the general solution method applicable to the three dimensional problems of the general shape seem to be under investigation with limited success [30]-[31].

3. GEOMETRIES OF INTEREST

Typical dimensions of the elements of interest are 2 x 20 μm. The magnetic layers of the elements are made from 150 - 250 $\mathring{A}$ thick permalloy ($Ni_{80}Fe_{20}$) or ternary alloy ($Ni_{65}Fe_{15}Co_{20}$) for minimum magnetostriction. These magnetic layers are separated by 50 - 150 $\mathring{A}$ thick nonmagnetic layers for which Ta is commonly used. The elements can be divided into two different types depending upon the alignment of the easy axis in the elements. The elements in which the easy axis is along the long dimension are called longitudinal elements and the elements whose easy axis is along the short dimension are called transverse elements. In this chapter the qualitative description of these elements will be presented along with the derivation of the 2-dimensional micromagnetic equation for each case.

3.1. Longitudinal Elements

The general shape of the longitudinal elements is depicted in Figure 3.1 [32]. Such elements can serve as memory elements and MR sensors as discussed earlier. Two external fields should be identified for the analysis of the elements. The external field parallel to the easy axis is called the longitudinal field (word field) and is supplied by the current of the word line. The field along the hard axis is generated from the sense current of the element itself and is called the transverse field (sense

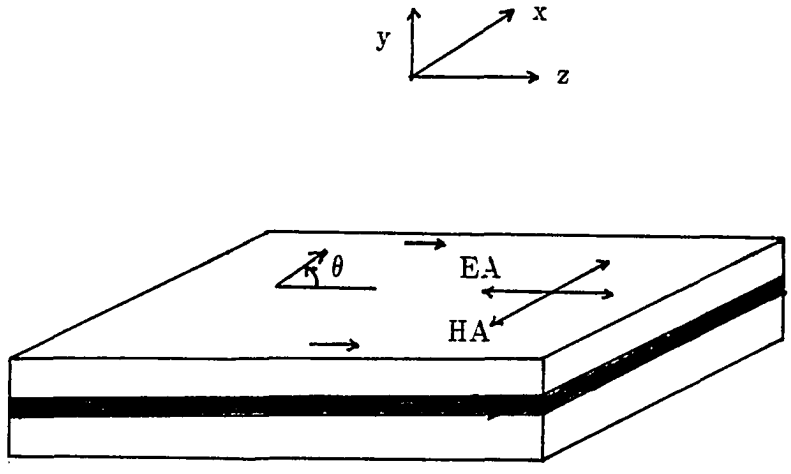

Figure 3.1: Longitudinal elements

field). The characteristics of the elements can be analyzed by investigating the output response. Figure 3.2 show the output voltage as the function of longitudinal field for a fixed transverse field. As shown in Figure 3.2, when we increase the longitudinal field starting from point A we meet the first switching point B.

It is known that the value of the point B is the function of both the longitudinal field and the transverse field and this function can be depicted as a curve whose shape is very similar to the Stoner-Wohlfarth switching astroid [33]. Furthermore, it has been shown that the thinner magnetic layer switches first in this type of element [34]. Since the switching mechanism of the Stoner-Wohlfarth astroid is coherent rotation, we can conclude that the switching of the point B is accomplished by the coherent rotation of magnetization at the interior of the thinner layer. After passing point B, two pseudo Néel walls are formed in the thinner layer of the elements since the edge magnetization of the elements are very strongly pinned at the edge. When

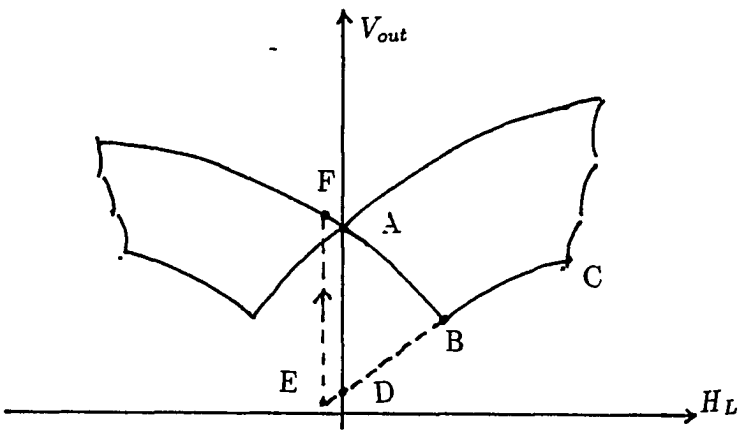

Figure 3.2: Response of longitudinal element

we further increase the longitudinal field to point C, we can observe another type of switching. Since the switching value at point C is independent of the transverse field, we can conclude that the switching is accomplished by wall motion as further evidenced by the Barkhausen noise. The Barkhausen noise is depicted as the discrete jumps starting from point C in Figure 3.2.

If the longitudinal field is turned off between the points B and C, the two possible final states are A and D depending upon the width of the elements [35]. If the width of the element is large enough to support the two paired Néel wall, point D will be the final point. Otherwise, the annihilation of the paired Néel walls will lead to the starting point A. At point D the application of a slight negative longitudinal field can annihilate the paired Néel walls resulting in the switching from E to F in Figure 3.2. This implies the possibility of two different modes of memory operation for this type of element. In the first mode the 1-state is assigned

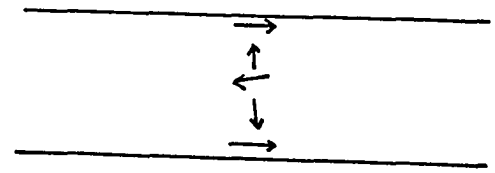

(a) 1-state

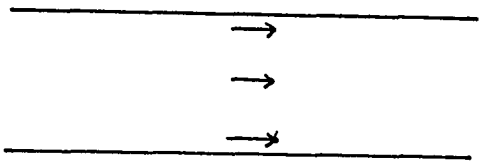

(b) 0-state

Figure 3.3: States of longitudinal element with walls

to the paired Néel wall state and 0-state is assigned to the wall-free state as shown in Figure 3.3. In the other mode two wall-free states are used for the two different states as shown in Figure 3.4.

The problems associated with the longitudinal mode elements as memory cells are:

1. For the memory mode shown in Figure 3.3, the width of the element should be large enough to support the two Néel walls.

2. For the memory mode shown in Figure 3.4, a large word current is required to change the pinned magnetization of the edge for write operation.

Because of these problems, this elements are currently investigated only for the applications as MR sensors.

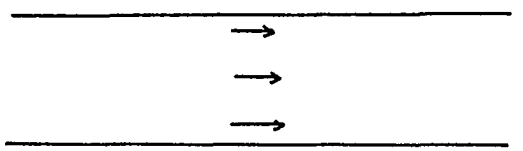

(a) 1-state

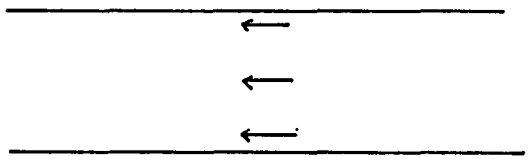

(b) 0-state

Figure 3.4: States of longitudinal element without walls

3.2. Transverse Mode

The easy axis of transverse mode elements lies along their short dimension [36]. The general shape of the element is shown in Figure 3.5 and the approximate magnetization distribution of the top and bottom layers at zero external field are depicted in Figure 3.6. which shows that the magnetization of the top layer is almost opposite in direction to that of the bottom layer at the middle of the element.

Thus, the strong magnetostatic coupling of the top and bottom layers decreases the troublesome magnetostatic energy of the element considerably even at a zero external field condition. For the analysis of its operation the output response of the transverse element is drawn in Figure 3.7 as a function of word field (transverse field) for a fixed sense field (longitudinal field).

Here, the word field is unidirectional and the sense field is bidirectional. If the

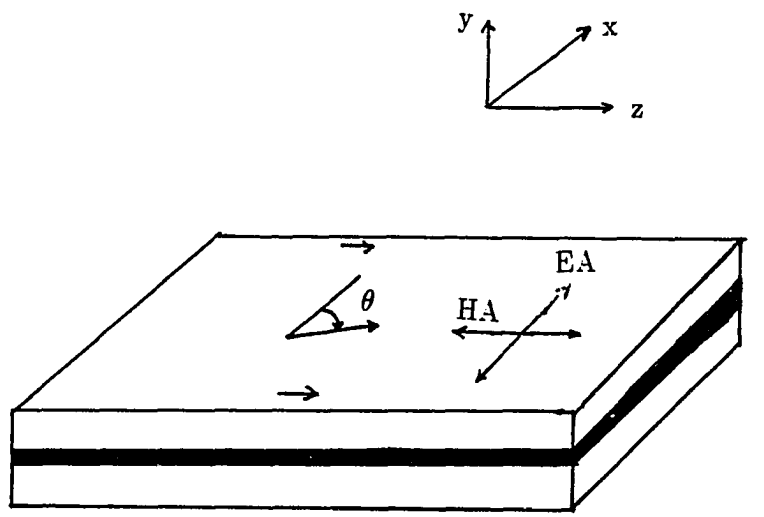

Figure 3.5: Transverse element

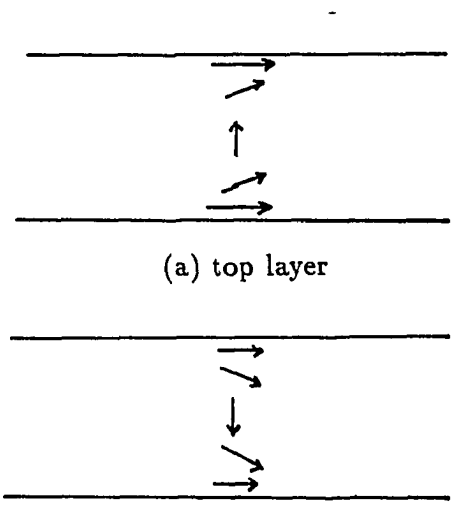

Figure 3.6: Magnetization of Transverse element

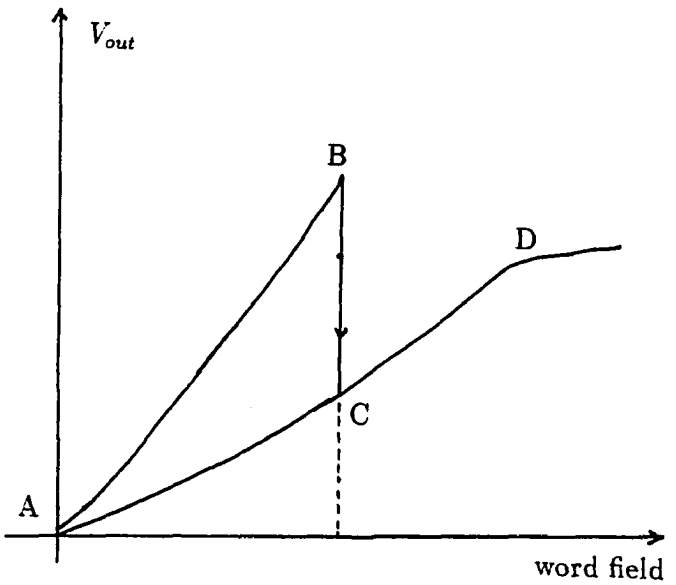

Figure 3.7: Output response of transverse element

sense current is applied in the direction which supports the present magnetization, the output response follows the A-C-D curve. In this case the word field which induces the rotation of the magnetization to the easy axis is resisted by the sense field. As a result, the slope of the curve A-D has a low value. On the other hand when the sense current is applied such that it opposes the original magnetization distribution, the output response follows the A-B curve. In this case, the sense field as well as the word field tends to rotate the magnetization into the easy axis, resulting in the output response following the steeper slop A-B. The further increase of word field beyond the point B induces switching, shown as the transition from B to C in Figure 3.7. In transverse elements, the switching of only one layer means that the magnetization of the switched layer is in the same direction as that

of the other layer at the middle of the element. As a result, the magnetostatic energy is increased. This increased magnetostatic energy enhances chances of the switching of the other layer. Thus, the switching of the both layers is accomplished almost simultaneously shown as the transition from B to C in Figure 3.7. Currently, extensive research on this type of element is under way.

3.3. Two-dimensional Micromagnetic Equations

In this section, the 2-dimensional micromagnetic equations which can be used to describe the magnetization distribution of the double-layered thin film elements will be derived from the 3-dimensional micromagnetic equations shown as Equation (2.31) and (2.32) under the following assumptions.

1. The variation of the in-plane component of the magnetization $\vec{M}$ in the thickness of the layers (y-direction) is assumed to be zero because of the exchange energy and the demagnetizing energy.

2. Y-directional contributions of the effective fields are ignored.

3. The fields arising from the sense current and word current is assumed to be constant throughout the element.

From assumption 1, the unit magnetization vector $\vec{m}$ of the longitudinal element becomes Equation (3.1).

$$\vec{m} = \sin\theta\vec{x} + \cos\theta\vec{z} \tag{3.1}$$

where θ is the angle between the magnetization and the easy axis as shown in Figure 3.1. Since the double derivatives of the $\sin\theta$ and $\cos\theta$ are given as Equations (3.2)

and (3.3), The $\nabla^2\vec{m}$ is given as Equation (3.4).

$$\frac{\partial^2}{\partial x^2}(\sin\theta) = -\sin\theta\left(\frac{\partial\theta}{\partial x}\right)^2 + \cos\theta\left(\frac{\partial^2\theta}{\partial x^2}\right) \tag{3.2}$$

$$\frac{\partial^2}{\partial x^2}(\cos\theta) = -\cos\theta\left(\frac{\partial\theta}{\partial x}\right)^2 - \sin\theta\left(\frac{\partial^2\theta}{\partial x^2}\right) \tag{3.3}$$

$$\begin{aligned}\nabla^2\vec{m} = &\left[-\sin\theta\left(\left(\frac{\partial\theta}{\partial x}\right)^2 + \left(\frac{\partial\theta}{\partial z}\right)^2\right) + \cos\theta\left(\left(\frac{\partial\theta}{\partial x}\right)^2 + \left(\frac{\partial\theta}{\partial z}\right)^2\right)\right]\vec{x} \\ &+\left[-\cos\theta\left(\left(\frac{\partial\theta}{\partial x}\right)^2 + \left(\frac{\partial\theta}{\partial z}\right)^2\right) - \sin\theta\left(\left(\frac{\partial\theta}{\partial x}\right)^2 + \left(\frac{\partial\theta}{\partial z}\right)^2\right)\right]\vec{z}\end{aligned} \tag{3.4}$$

From Equation (3.1) and Equation (3.4), we can get Equation (3.5).

$$\vec{m}\times\nabla^2\vec{m} = \left(\frac{\partial^2\theta}{\partial x^2} + \frac{\partial^2\theta}{\partial z^2}\right)\vec{y} \tag{3.5}$$

Equation (3.5) represents the contribution of the exchange energy to the micromagnetic equation.

From assumptions 2 and 3 we can write $\vec{H}_d$ and $\vec{H}_o$ as Equations (3.6) and (3.7), respectively.

$$\vec{H}_d = H_{dx}\vec{x} + H_{dz}\vec{z} \tag{3.6}$$

$$\vec{H}_o = H_{ox}\vec{x} + H_{oz}\vec{z} \tag{3.7}$$

Thus, the contributions of $\vec{H}_0$ and $\vec{H}_d$ to the micromagnetic equation are given as Equation (3.8).

$$\vec{m}\times\left(\vec{H}_d + \vec{H}_o\right) = \left[\left(H_{dx} + H_{ox}\right)\cos\theta - \left(H_{dz} + H_{oz}\right)\sin\theta\right]\vec{y} \tag{3.8}$$

Next, the uniaxial anisotropy energy density, assuming the easy axis is the z-direction, can be expressed as Equation (3.9).

$$w_a = \frac{H_k M_s}{2}\sin^2\theta = \frac{H_k M_s}{2}\left(1-\gamma^2\right) \tag{3.9}$$

where γ is the z-directional cosine. Since the variation on w_a is given as

$$\begin{aligned}\frac{\partial w_a}{\partial \vec{m}} &= \frac{\partial w_a}{\partial \alpha}\vec{x} + \frac{\partial w_a}{\partial \beta}\vec{y} + \frac{\partial w_a}{\partial \gamma}\vec{z} \\ &= -H_k M_s \cos\theta \vec{z}. \end{aligned} \tag{3.10}$$

Then, from Equation (3.10) and Equation (3.1) we get Equation (3.11) which is the contribution of the anisotropy energy to the micromagnetic equation.

$$\vec{m} \times \left(\frac{-\partial w_a}{\partial \vec{m}}\right) = -H_k M_s \cos\theta \sin\theta \vec{y} \tag{3.11}$$

By summing up Equation (3.5), Equation (3.8) and Equation (3.11) we get the 2-dimensional micromagnetic equation for the longitudinal elements as Equation (3.12).

$$\begin{aligned}\frac{2A}{M_s}\left(\frac{\partial^2\theta}{\partial x^2} + \frac{\partial^2\theta}{\partial z^2}\right) + (H_{dx} + H_{ox})\cos\theta - (H_{dz} + H_{oz})\sin\theta \\ -H_k \sin\theta\cos\theta = 0 \end{aligned} \tag{3.12}$$

The boundary condition of the longitudinal element can be derived from Equation (2.32) in the following way. Since the outwardly normal vector $\vec{n} = \cos\theta\vec{x} - \sin\theta\vec{z}$ and

$$\frac{\partial F}{\partial n} = \nabla F \cdot \vec{n},$$

we can express $\partial\vec{m}/\partial n$ as Equation (3.13).

$$\begin{aligned}\frac{\partial \vec{m}}{\partial n} &= \left(\cos\theta\frac{\partial\theta}{\partial x}, 0, \cos\theta\frac{\partial\theta}{\partial z}\right)\cdot(\cos\theta, 0, -\sin\theta)\,\vec{x} \\ &+ \left(-\sin\theta\frac{\partial\theta}{\partial x}, 0, -\sin\theta\frac{\partial\theta}{\partial z}\right)\cdot(\cos\theta, 0, -\sin\theta)\,\vec{z} \\ &= \left(\cos^2\theta\frac{\partial\theta}{\partial x} - \cos\theta\sin\theta\frac{\partial\theta}{\partial z}\right)\vec{x} \\ &+ \left(\sin^2\theta\frac{\partial\theta}{\partial z} - \sin\theta\cos\theta\frac{\partial\theta}{\partial x}\right)\vec{z} \end{aligned} \tag{3.13}$$

Thus, a boundary condition for the longitudinal mode micromagnetic equation is given by Equation (3.14).

$$\vec{m} \times \frac{\partial \vec{m}}{\partial n} = \sin\theta \frac{\partial \theta}{\partial z} - \cos\theta \frac{\partial \theta}{\partial x} = 0 \tag{3.14}$$

Generally, the surface anisotropy term in Equation (2.32) is ignored and Equation (3.14) serves as the boundary condition [23]. However, we can get simpler boundary condition by using the empirical fact that the magnetization is pinned at the edge of the elements. The boundary condition thus obtained can be expressed as Equation (3.15).

$$\vec{n} \cdot \vec{m} = 0 \tag{3.15}$$

Here, the Equation (3.15) will be used for the boundary condition of Equation (3.12). The comparison of the results obtained by using Equation (3.15) and Equation (3.14) remains as future work.

For transverse elements the unit magnetization vector $\vec{m}$ becomes

$$\vec{m} = \cos\theta \vec{x} + \sin\theta \vec{z} \tag{3.16}$$

where θ is the angle between the magnetization and the easy axis of the transverse element as shown in Figure 3.4. Using the same procedures as for Equations (3.2) - (3.4), we obtain

$$\vec{m} \times \nabla^2 \vec{m} = -\left(\frac{\partial^2 \theta}{\partial x^2} + \frac{\partial^2 \theta}{\partial z^2}\right) \vec{y}. \tag{3.17}$$

Equation (3.17) is the contribution of the exchange energy to the micromagnetic equation of the transverse elements.

The contributions from the external field and the demagnetizing field can be written as Equation (3.18).

$$\vec{m} \times \left(\vec{H}_d + \vec{H}_o\right) = \left((H_{dx} + H_{ox})\sin\theta - (H_{dz} + H_{oz})\cos\theta\right)\vec{y} \tag{3.18}$$

where $\vec{H}_d$ and $\vec{H}_o$ are defined in Equations(3.6) and (3.7), respectively.

In the transverse element the easy axis is along the x-direction. Therefore, the anisotropy energy density w_a is given by the following equation.

$$w_a = \frac{H_k M_s}{2} \sin^2\theta = \frac{H_k M_s}{2}\left(1-\alpha^2\right) \tag{3.19}$$

where α is the x-directional cosine.

The variation on Equation (3.19) leads to Equation (3.20).

$$\begin{aligned}\frac{\partial w_a}{\partial \vec{m}} &= \frac{\partial w_a}{\partial \alpha}\vec{x} + \frac{\partial w_a}{\partial \beta}\vec{y} + \frac{\partial w_a}{\partial \gamma}\vec{z} \\ &= -H_k M_s \cos\theta \vec{x}\end{aligned} \tag{3.20}$$

Then, from Equation (3.16) and Equation (3.20) the contribution of the anisotropy energy term is given by Equation (3.21).

$$\vec{m} \times \frac{\partial w_a}{\partial \vec{m}} = H_k M_s \sin\theta\cos\theta\vec{y} \tag{3.21}$$

By collecting on Equations (3.17), (3.18) and (3.21) we have

$$\begin{aligned}\frac{2A}{M_s}\left(\frac{\partial^2\theta}{\partial x^2}+\frac{\partial^2\theta}{\partial z^2}\right) - (H_{dx}+H_{ox})\sin\theta + (H_{dz}+H_{oz})\cos\theta \\ -H_k \sin\theta\cos\theta\vec{y} = 0.\end{aligned} \tag{3.22}$$

Equation (3.22) is the micromagnetic equation for transverse elements.

The outwardly normal vector is given as $\vec{n} = \sin\theta\vec{x} - \cos\theta\vec{z}$ for the transverse elements. Thus, the boundary condition of the micromagnetic equation for transverse mode is obtained in the following way. Since the derivative of $\vec{m}$ with respect to $\vec{n}$ is given by Equation (3.23),

$$\begin{aligned}\frac{\partial \vec{m}}{\partial n} &= \left(-\sin\theta\frac{\partial\theta}{\partial x}, 0, -\sin\theta\frac{\partial\theta}{\partial z}\right)\cdot(\sin\theta, 0, -\cos\theta)\,\vec{x} \\ &+ \left(\cos\theta\frac{\partial\theta}{\partial x}, 0, \cos\frac{\partial\theta}{\partial z}\cdot(\sin\theta, 0, -\cos\theta)\,\vec{z}\right. \\ &= \left(-\sin^2\theta\frac{\partial\theta}{\partial z} + \sin\theta\cos\theta\frac{\partial\theta}{\partial z}\right)\vec{x} \\ &+ \left(-\cos^2\theta\frac{\partial\theta}{\partial z} + \sin\theta\cos\theta\frac{\partial\theta}{\partial x}\right)\vec{z} \qquad (3.23)\end{aligned}$$

then, the boundary condition is given by Equation (3.24).

$$\vec{m}\times\frac{\partial\vec{m}}{\partial n} = \cos\theta\frac{\partial\theta}{\partial z} - \sin\theta\frac{\partial\theta}{\partial x} = 0 \qquad (3.24)$$

However, the empirical boundary condition given in Equation (3.15) will be used instead of Equation (3.24) for the transverse element, also.

So far, a practical method which can be used to calculate the demagnetizing field $\vec{H}_d$ has not been discussed. The demagnetizing field has the long range coupling effect between segments. Moreover, the top and bottom layers interact only through demagnetizing field effects. The calculation of demagnetizing field imposes the most challenging problem for the solution of the micromagnetic equation, and this issue will be discussed in Chapter 4.

4. DEMAGNETIZING FIELDS

As mentioned in Section 3.3, the determination of the demagnetizing field $\vec{H}_d$ is the most difficult part of solving the micromagnetic equation. To get the demagnetizing field at one point of the element, the magnetization distribution of the whole element must be known. On the other hand, the magnetization distribution can not be calculated without the knowledge of the demagnetizing field. Thus, calculation of the magnetization distribution and the demagnetizing field constitutes a circular problem. For this reason, an iterative method starting from a well-guessed magnetization distribution is employed to solve the micromagnetic equation.

Another problem associated with the demagnetizing field calculation is the excessive computation time required to calculate the demagnetizing fields. For example, assume that we have a element consisting of n segments. To compute the demagnetizing field of a segment, the contributions from the $n-1$ segments should be calculated. Thus, the computation time required to calculate the demagnetizing fields of all segments for one iteration is proportional to n^2, which discourages fine segmentation of the elements. In this chapter, several ways of calculating the demagnetizing fields will be presented along with a brief comparison of their accuracy.

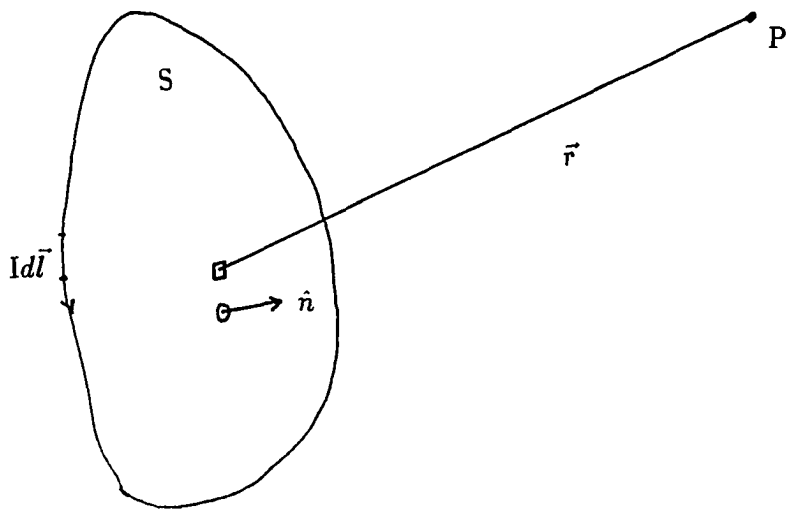

Figure 4.1: Dipole Moment

4.1. Dipole Moment Method

The magnetization $\vec{M}$ in the ferromagnetic material can be interpreted as the volume average of the dipole moment $\vec{m}$. Therefore, the magnetic field generated by the dipole moment can be used directly for the calculation of the demagnetizing field [37]. The dipole moment can be represented by the current loop which carries constant current I as depicted in Figure 4.1.

Here, the dipole moment is defined as

$$\vec{p} = I \int d\vec{S} = IS\vec{n} \tag{4.1}$$

where S is the surface area of the current loop and $\vec{n}$ is the outward normal unit vector of the surface S. The vector potential $\vec{A}$ and scalar potential Φ can be expressed as Equations (4.2) and (4.3) respectively.

$$\vec{A} = I \oint \frac{\vec{dl}}{r} = I \int \frac{\vec{n} \times \hat{r}}{r^2} dS \tag{4.2}$$

$$\Phi = I \int \frac{\vec{n} \cdot \hat{r}}{r^2} dS \tag{4.3}$$

where $\hat{r}$ is the unit vector of the distance vector $\vec{r}$ and r is the magnitude of $\vec{r}$. When all the distance vectors from the surface S to the point P can be approximated by one representative distance vector $\vec{r}$, the Equations (4.1) and (4.2) become,

$$\vec{A} = -\frac{\hat{r}}{r^2} \times \left(I \int \vec{n} dS \right) = \frac{\vec{p} \times \hat{r}}{r^2} \tag{4.4}$$

$$\Phi = \frac{\hat{r}}{r^2} \cdot \left(I \int \vec{n} dS \right) = \frac{\hat{r} \cdot \vec{p}}{r^2}. \tag{4.5}$$

Under the assumption that the $\vec{p}$ is located at an infinitesimally small region which can be treated as a point, the ferromagnetic material can be modelled as the collection of the points which represent dipole moment $\vec{p}$. Then, the area not occupied by the point dipole moments can be regarded as the magnetization free space where $\vec{H} = \vec{B}$. Then, the demagnetizing field at point $\vec{r}$ which is in free space is

$$\begin{aligned} \vec{H}_d &= \vec{\nabla} \times \vec{A} = -\nabla \Phi \\ &= \frac{-\vec{p} + 3\left(\vec{p} \cdot \hat{r}\right) \hat{r}}{r^3}. \end{aligned} \tag{4.6}$$

The demagnetizing field of a segment i in the element can be computed by adding the contributions from the rest of the element as shown in Equation (4.7).

$$\vec{H}_i = \sum_{j \neq i} \frac{-\vec{p_j} + \left(\vec{p_j} \cdot \hat{r_{ij}}\right) \hat{r_{ij}}}{{r_{ij}}^3} \tag{4.7}$$

where r_{ij} is the distance between points i and j and $\hat{r_{ij}}$ is its unit vector and $\vec{p_j}$ is the magnetic dipole of point j. Since $\vec{p} = \vec{M} \cdot \nabla v$ in the ferromagnetic material Equation (4.7) becomes,

$$\vec{H}_i = \sum_{j} \frac{-\left(\vec{M_j} \nabla v_j\right) + \left(\vec{M_j} \cdot \hat{r_{ij}}\right) \nabla v_j \hat{r_{ij}}}{{r_{ij}}^3} \tag{4.8}$$

where ∇v_j is the volume represented by dipole p_j.

4.2. Scalar Potential Method

The exact expression for the demagnetizing field can be obtained by manipulating the scalar potential which is derived from the volume change density $-\nabla \cdot \vec{M}$ and the surface charge density $\vec{M} \cdot \vec{n}$ as shown in Equation (4.9) [20]-[21].

$$\Phi(\vec{r}) = \int \frac{-\nabla' \cdot \vec{M}(\vec{r}')}{|\vec{r} - \vec{r}'|} dv' + \int \frac{\vec{n}' \cdot \vec{M}(\vec{r}')}{|\vec{r} - \vec{r}'|} dS' \tag{4.9}$$

where $\vec{r}'$ is the position vector of the magnetic free pole and $\vec{r}$ is the position vector of the point of interest and v' and S' represents the volume and surface of the magnetic poles, respectively. Since the position vectors $\vec{r}$ and $\vec{r}'$ are independent of each other, the volume integral term in the Equation (4.9) becomes

$$\int \frac{-\nabla' \cdot \vec{M}(\vec{r}')}{|\vec{r} - \vec{r}'|} dv' = -\nabla' \cdot \int \frac{\vec{M}(\vec{r}')}{|\vec{r} - \vec{r}'|} dv' + \nabla \cdot \int \frac{\vec{M}(\vec{r})'}{|\vec{r} - \vec{r}'|} dv'. \tag{4.10}$$

Furthermore, the application of the divergence theorem to the surface integral term in Equation (4.9) yields

$$\int \frac{\vec{n}' \cdot \vec{M}(\vec{r}')}{|\vec{r} - \vec{r}'|} dS' = \nabla' \cdot \int \frac{\vec{M}(\vec{r}')}{|\vec{r} - \vec{r}'|} dv \tag{4.11}$$

Thus, Equation (4.9) becomes

$$\Phi(\vec{r}) = \vec{\nabla} \cdot \int \frac{\vec{M}(\vec{r}')}{|\vec{r} - \vec{r}'|} dv' \tag{4.12}$$

From the relation $\vec{H}_d = -\nabla \cdot \Phi(\vec{r})$ and the Equation (4.12) we have,

$$\vec{H}_d(\vec{r}) = -\vec{\nabla} \left[\vec{\nabla} \cdot \int \frac{\vec{M}(\vec{r}')}{|\vec{r} - \vec{r}'|} dv' \right]$$

$$= \nabla^2 \int \frac{\vec{M}(\vec{r}')}{|\vec{r} - \vec{r}'|} dv' - \nabla \times \nabla \times \int \frac{\vec{M}(\vec{r}')}{|\vec{r} - \vec{r}'|} dv' \tag{4.13}$$

Since

$$\nabla^2 \left(\frac{1}{\mid \vec{r} - \vec{r}' \mid} \right) = -4\pi\delta^3 (\vec{r} - \vec{r}')$$

where $\delta^3 (\vec{r} - \vec{r}')$ is the delta function in 3 dimensions, Equation (4.13) can be transformed into Equation (4.14).

$$\vec{H}_d (\vec{r}) = -4\pi\vec{M} (\vec{r}) - \nabla \times \nabla \times \int \frac{\vec{M} (\vec{r}')}{\mid \vec{r} - \vec{r}' \mid} dv' \tag{4.14}$$

Equation (4.14) is the exact expression of the demagnetizing field and was used for 1-dimensional calculation [20]. However, the calculation of the demagnetizing field based on Equation (4.14) requires the evaluation of a triple integral which is generally a very complicated process for practical use.

4.3. Energy Method

This method was first used by Brown and Labonte for the 1-dimensional [28] treatment of the Bloch wall. Recently, this method was generalized by Schabes and Aharoni for three-dimensional problems [38].

This method starts from the assumption that the sample consists of n cubic cells in which the magnetization is homogeneous. Thus, all the magnetic free poles appear at the boundaries of the cubes as surface charge. Then, the magnetostatic energy of cube i is given by Equation (4.15).

$$W_i = \int \left[\sum_{j \neq i} \sigma_i \Phi_{ij} \right] dS_i \tag{4.15}$$

where σ_i is the surface charge of position i and Φ_{ij} is the scalar potential at position i due to the surface charge of position j. Φ_{ij} is given by

$$\Phi_{ij} = \int \frac{\sigma_j}{\mid \vec{r_i} - \vec{r_j} \mid} dS_j. \tag{4.16}$$

Here, the demagnetizing field at position i is given by Equation (4.17).

$$\vec{H}_{di} = -\frac{1}{M_s v}\frac{\partial W_{di}}{\partial \vec{m}} = -\frac{1}{M_s v}\left[\frac{\partial W_{di}}{\partial \alpha}\vec{x} + \frac{\partial W_{di}}{\partial \beta}\vec{y} + \frac{\partial W_{di}}{\partial \gamma}\vec{z}\right] \tag{4.17}$$

where M_s is the saturation magnetization and v is the volume of the cell and α, β, γ are direction cosines.

4.4. Surface Charge Method

Since the exact expressions obtained in Sections 4.2 and 4.3 are very complicated, an approximation method which gives a relatively simple and accurate expression has been adopted for the current discussion. The same surface poles are defined as in Section 4.3. However, the demagnetizing field is directly computed from the surface poles instead of going through the calculation of energy. Therefore, this method can be regarded as a point sample method while the method discussed in Section 4.3 can be viewed as a volume averaging method.

As mentioned before the demagnetizing field can be computed from the scalar potential as in Equation (4.18).

$$\begin{aligned}\vec{H}_d(\vec{r}) = -\nabla\Phi(r) &= -\nabla\int \frac{\sigma(\vec{r}')}{|\vec{r}-\vec{r}'|}dS' \\ &= \int \frac{\sigma(\vec{r}')(\vec{r}-\vec{r}')}{|\vec{r}-\vec{r}'|^3}dS'\end{aligned} \tag{4.18}$$

If we assume that the surface charge $\sigma(\vec{r}')$ is constant all over the surface and is located at the origin and $\vec{r} = a\vec{x} + b\vec{y} + c\vec{z}$ as shown in Figure 4.2, then, Equation (4.18) becomes

$$\begin{aligned}\vec{H}_d(a,b,c) = \sigma \int_{z=-l_z}^{l_z}\int_{y=-l_y}^{l_y} &\frac{a\vec{x} + (b-y)\vec{y} + (c-z)\vec{z}}{\left[a^2 + (b-y) + (c-z)^2\right]^{\frac{3}{2}}}dydz. \\ &= H_{dx}\vec{x} + H_{dy}\vec{y} + H_{dz}\vec{z}\end{aligned} \tag{4.19}$$

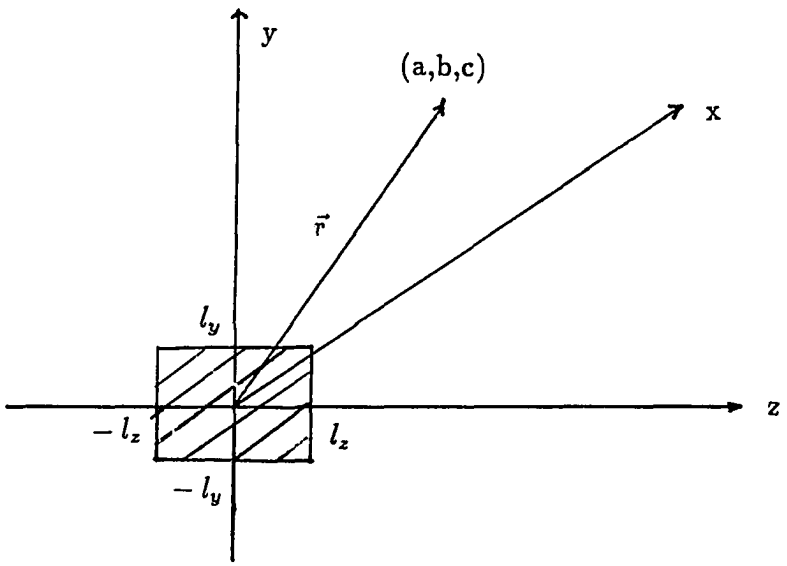

Figure 4.2: Demagnetizing field from the surface charge

After a few arithmetic operations we can derive the following relations.

$$
\begin{aligned}
H_{dx}(a,b,c) = \sigma \Bigg[& \tan^{-1}\left(\frac{(b-l_y)(c-l_z)}{a\sqrt{a^2+(b-l_y)^2+(c-l_z)^2}}\right) \\
& + \tan^{-1}\left(\frac{(b+l_y)(c-l_z)}{a\sqrt{a^2+(b+l_y)^2+(c-l_z)^2}}\right) \\
& + \tan^{-1}\left(\frac{(b-l_y)(c+l_z)}{a\sqrt{a^2+(b-l_y)+(c+l_z)^2}}\right) \\
& + \tan^{-1}\left(\frac{(b+l_y)(c+l_z)}{a\sqrt{a^2+(b+l_y)+(c+l_z)^2}}\right)\Bigg]
\end{aligned}
\qquad (4\ :0)
$$

$$H_{dz}(a,b,c) = \sigma \left[\ln \frac{\left(\sqrt{{K_2}^2 + (b+l_y)^2} + (b+l_y)\right)}{\left(\sqrt{{K_2}^2 + (b-l_y)^2} + (b-l_y)\right)} + \ln \frac{\left(\sqrt{{K_1}^2 + (b-l_y)^2} + (b-l_y)\right)}{\left(\sqrt{{K_1}^2 + (b+l_y)^2} + (b+l_y)\right)} \right] \tag{4.21}$$

where ${K_1}^2 = a^2 + (c+l_z)^2$ and ${K_2}^2 = a^2 + (c-l_z)^2$.

Since elements are very thin, the y-component of the demagnetizing field is ignored. For numerical analysis Equations (4.20) and (4.21) should be digitized. Note that the digitized versions of Equations (4.20) and (4.21) need to be evaluated just $n-1$ times for n cells, since we have $n-1$ different distance vectors between the surface poles and the point of interest.

To complete this discussion the values of the demagnetizing fields resulting from the methods discussed so far will be compared. It is assumed that we have an array of identical cubes whose magnetizations are saturated in one direction. Note that the methods of Sections 4.2 and 4.3 should give the same result. The ratios of the demagnetizing fields r_1 and r_2 are defined as follows :

$$r_1 = \frac{Dipole\ \ method}{Energy\ \ method}$$

$$r_2 = \frac{Surface\ \ pole\ \ method}{Energy\ \ method}$$

The values of r_1 and r_2 are listed in Table 4.1, in which the values of n designate the digitized distance between the source cell and the cell of interest.

Table 4.1: Ratios

n	r_1[31]	r_2
1	1.1788	0.9983
2	1.0243	1.0111
3	1.0052	1.0026
4	1.0017	1.0009

As shown in Table 4.1 the value of r_1 and r_2 approach 1 as the value of n increases. Another thing to note from Table 4.1 is that the surface pole method differs from the energy method by less than 1.2 % while the dipole method gives almost an 18 % difference. Therefore, it can be concluded that the surface pole method is a good compromise between complexity and accuracy in calculating demagnetizing fields.

5. NUMERICAL ANALYSIS

In this chapter a numerical method used to solve the 2-dimensional micromagnetic Equations (3.12) and (3.22) will be discussed. The boundary condition of these equations is given in Equation (3.15) and the surface pole method described in Section 4.5 is used to complete the demagnetizing fields.

Generally, the dimension of the element is 2 x 20 μm with 150 $\mathring{A}$ thick magnetic layers and a 50 $\mathring{A}$ thick nonmagnetic layer. The two different shapes of elements considered are rectangular and diamond as shown in Figure 5.1. Each shape is solved for both longitudinal mode and transverse mode elements. To solve the micromagnetic equations numerically, each magnetic layer is divided into 40 x 100 segments (500 x 2000$\mathring{A}$ for each segment). Since the direction of magnetization in each segment represents a variable of the micromagnetic equations, the number of variables is 8,000. Thus, the micromagnetic equations are equivalent to 8,000 simultaneous nonlinear equations which can be expressed by an 8,000 x 8,000 matrix. Since the demagnetizing field couples every variable in the element, this matrix becomes a full matrix. The nonlinearity of the simultaneous equations and the number of computations required to solve a 8,000 x 8,000 full matrix $\left(\cong 8,000^3\right)$ makes it almost impossible to solve the micromagnetic equations by this method. Therefore, an iteration method was adopted to solve the micromagnetic equation.

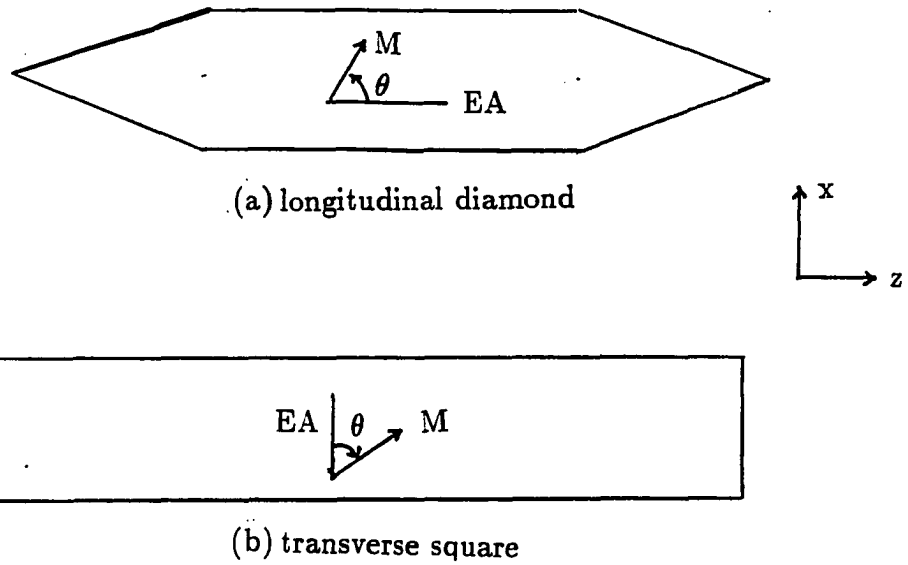

(a) longitudinal diamond

(b) transverse square

Figure 5.1: Various shapes of elements

One of the inherent advantages of the iteration method is that round-off error will be damped out as the iteration continues. The iteration starts from the initial guess which plays a very important role in getting the solution since the convergence itself as well as the speed of the convergence is dependent on it. As the initial guess the 1-dimensional model developed by Pohm et al. [36] is used. The details of this method will be described in Section 5.1. After the initial set-up is completed by the 1-dimensional method, 2-dimensional micromagnetic equations are solved by the point iteration method whose details are the subjects of Section 5.2.

5.1. 1-dimensional Model

At the middle of the elements the z-directional angle variation and the z-directional edge effect can be ignored since the z-directional length of the elements is relatively large ($20\mu m$). Therefore, the z-directional exchange energy term ($= d^2\theta/dz^2$) can be ignored. Moreover, the z-directional demagnetizing field can be obtained by an ellipsoidal approximation which is given by Equations (5.1) and (5.2).

$$H_{dz} \cong \frac{2\pi M_s}{p^2}(ln2p - 1) \tag{5.1}$$

$$P \cong \frac{l}{r} \cong \frac{l}{\sqrt{\frac{TW}{\pi}}} \tag{5.2}$$

where

M_s : Saturation magnetization (983 emu/cm^3)

l : Half length of elements (=10 μm)

T : Total thickness of magnetic layer (= 300 $\mathring{A}$)

W : width of the element (= 2 μm)

Thus, the approximate value of H_{dz} is 2.55 Oe for our case. The micromagnetic equations can be further simplified with the assumption that the top and bottom layers have the exactly opposite magnetic poles in the sandwich structured elements because of geometric symmetry.

Under the above assumption the x-direction demagnetizing fields can be expressed as an analytic expression by the following procedures. In the longitudinal element, the y-directional fields can be approximated by the Equation (5.3) because the opposite magnetic poles generated at the top and bottom layers are proportional

to the divergence of the magnetization $\vec{M}$.

$$H_y \cong 4\pi T \frac{d(\sin\theta)}{dx} \tag{5.3}$$

where T is the thickness of a magnetic layer (150 $\mathring{A}$). Since the magnetic fields of interest are generated only by the magnetization $\vec{M}$, we have Equation (5.4).

$$\oint \vec{H} \cdot d\vec{l} = 0 \tag{5.4}$$

When Equation (5.4) is applied on the closed path shown in Figure 5.2, the x-direction demagnetizing field of the longitudinal mode element is given by Equation (5.5).

$$H_{dx} = 2\pi M_s T s' \frac{d^2(\sin\theta)}{dx^2} \tag{5.5}$$

where s' is the effective separation distance between opposite magnetic poles and is given as 60 $\mathring{A}$ for this case.

By the same procedure we can prove easily that the x-direction demagnetizing field for the transverse mode element is given by Equation (5.6).

$$H_{dx} = 2\pi M_s s' \frac{d^2(\cos\theta)}{dx^2} \tag{5.6}$$

With the above approximations the 2-dimensional micromagnetic Equations (3.12) and (3.22) become

$$\left(\frac{2A}{M_s} + C\cos^2\theta\right)\frac{d^2\theta}{dx^2} - C\cos\theta\sin\theta\left(\frac{d\theta}{dx}\right)^2$$
$$= H_k\cos\theta\sin\theta - H_{ox}\cos\theta + (H_{oz} + 2.55)\sin\theta \tag{5.7}$$

$$\left(\frac{2A}{M_s} + C\sin^2\theta\right)\frac{d^2\theta}{dx^2} + C\cos\theta\sin\theta\left(\frac{d\theta}{dx}\right)^2$$
$$= H_k\cos\theta\sin\theta + H_{ox}\sin\theta - (H_{oz} + 2.55)\cos\theta \tag{5.8}$$

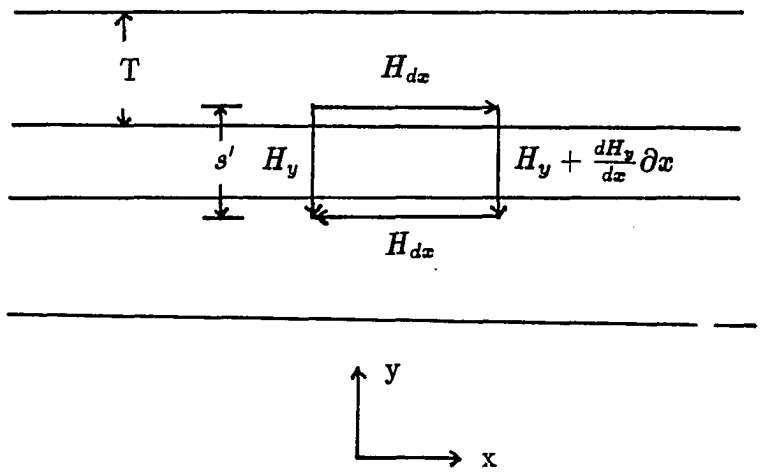

Figure 5.2: Analytic x-directional demagnetizing field

where C is given by Equation (5.9).

$$C = 2\pi M_s T s' \tag{5.9}$$

With the boundary condition that the magnetization is pinned at the edges of the element, Equations (5.8) and (5.9) represents a 1-dimensional boundary value problem which can be solved by any method applicable to such problems. Here, Euler's method was used to proceed from one point to the next point and the shooting method in which the first derivative of the starting point is adjusted according to the previous trial was used to satisfy the boundary condition. Typical results of these equations for the various external field conditions are shown in Figures 5.3 and 5.4 for the longitudinal mode and the transverse mode, respectively. H_l and H_t are the fields applied along the easy axis and the hard axis, respectively. X-axis is along the width of element and y-axis represents the angle of magnetization in

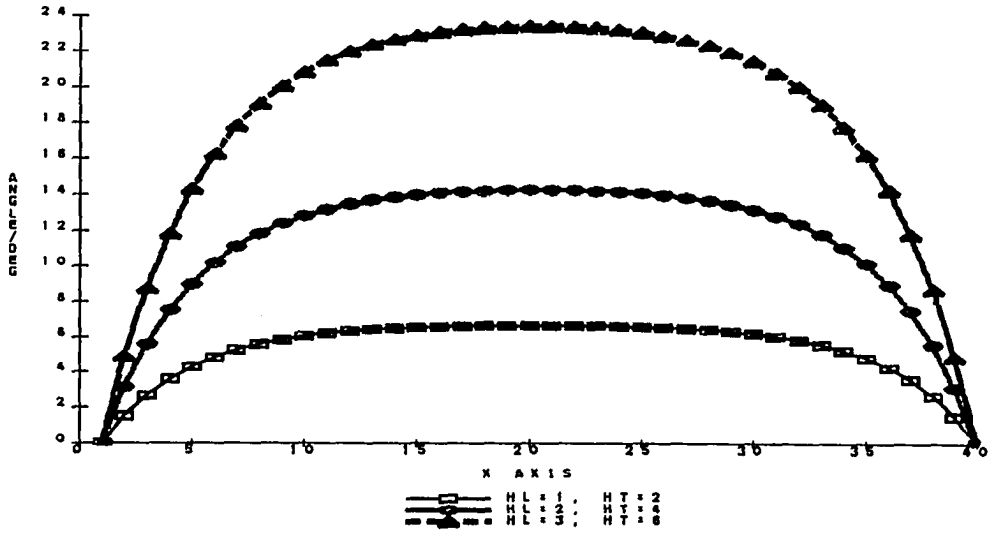

Figure 5.3: 1-dimensional solutions of longitudinal mode elements, units of x-axis and y-axis are 500 $\mathring{A}$ and 1°, respectively

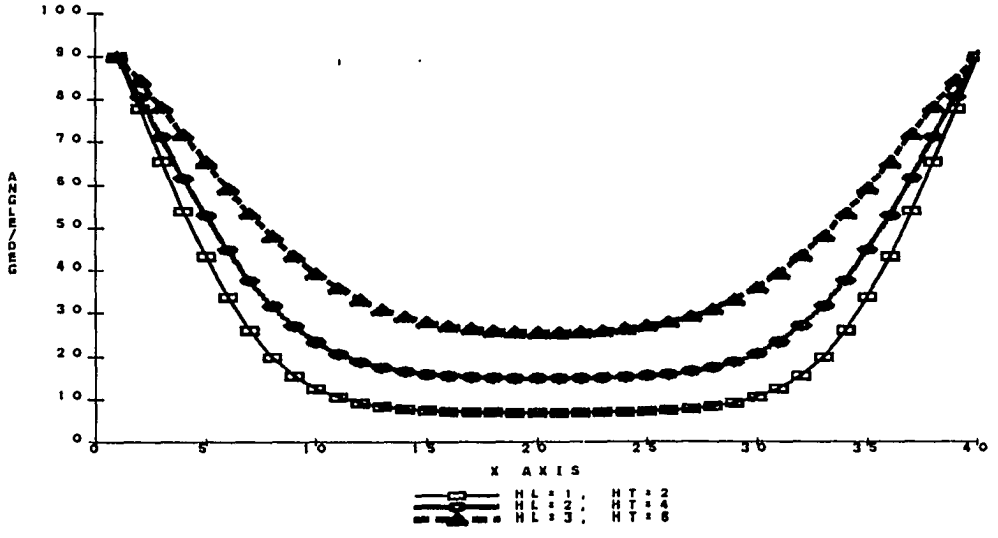

Figure 5.4: 1-dimensional solution of transverse mode elements, units of x-axis and y-axis are 500 $\mathring{A}$ and 1°, respectively

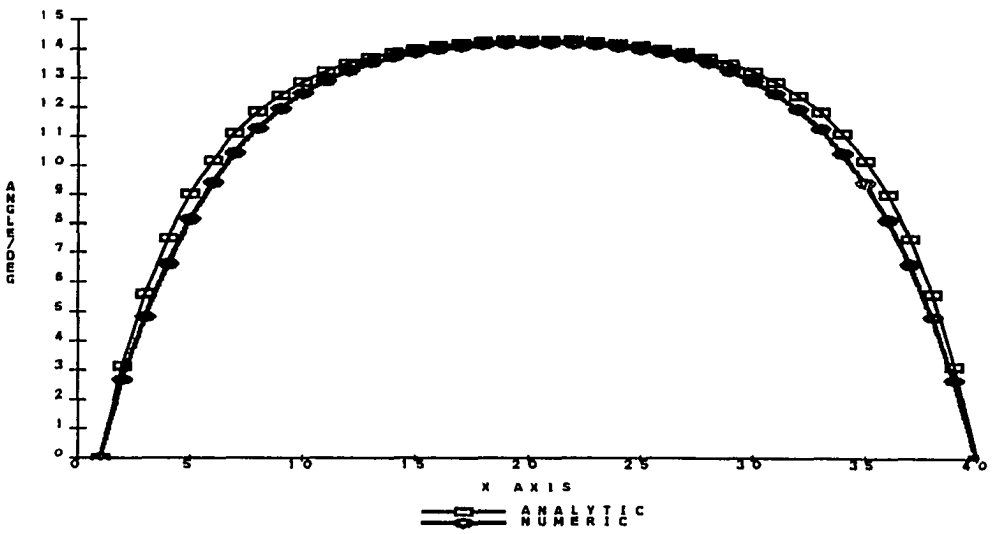

Figure 5.5: Comparison between analytic and numeric solutions of longitudinal mode elements, units of x-axis and y-axis are 500 $\mathring{A}$ and 1°, respectively

degree in these figures. The results of the analytic 1-dimensional equations are used as initial values for the solution of the numerical 1-dimensional equations in which the x-directional demagnetizing fields are calculated by the surface pole method instead of Equations (5.7) and (5.8). Figure 5.5 and 5.6 compares the solutions of the 1-dimensional analytic equation with those of the 1-dimensional numerical equation. As shown in those figures, the results are in close agreement.

The analytical Equations (5.7) and (5.8) were used successfully to predict the switching threshold of the elements. Generally, the energy of the memory elements can be described as having two stable states marked as points A and B which are separated by energy barrier marked by point C as shown in Figure 5.7. Thus, the 1-dimensional micromagnetic equation has two stable solutions which correspond to point A and B and one unstable solution corresponding to point C. Here, the

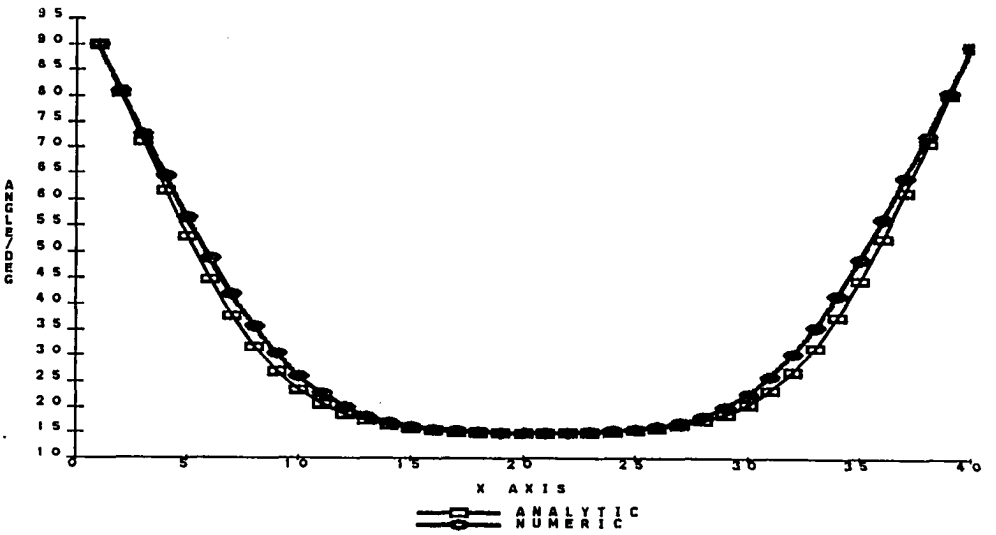

Figure 5.6: Comparison between analytic and numeric solutions of transverse elements, units of x-axis and y-axis are 500 $\mathring{A}$ and 1°, respectively

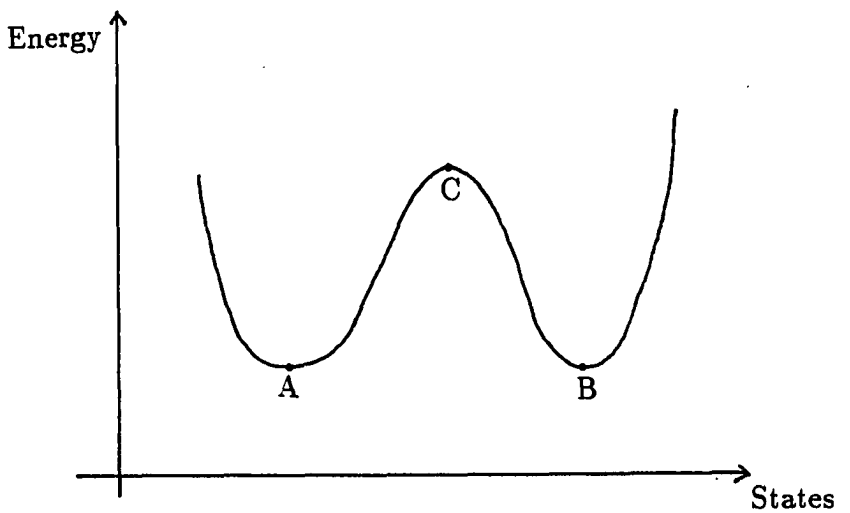

Figure 5.7: Energy states of memory elements

switching threshold of the element can be obtained by the following procedure. If the external fields are increased such that one stable condition is favored over the other, then the unfavored state disappears at some external field which is the switching threshold. Therefore, the switching threshold is obtained by finding the critical external field which separates the 1-solution state and the 3-solution state. The switching thresholds obtained by the above method are shown in Figure 5.8 along with the Stoner-Wohlfarth switching threshold. It was proved that the switching thresholds shown in Figure 5.8 match very well with the experimental values [39].

5.2. 2-dimensional Model

After the initial set-up is completed by using the 1-dimensional equations, the 2-dimensional Equations (3.12) and (3.22) are solved by the following methods. Since Equations (3.12) and (3.22) are elliptic equations, they can be written as

$$\frac{\partial^2 \theta_{i,j}}{\partial x^2} + \frac{\partial^2 \theta_{i,j}}{\partial z^2} = f\left(\theta_{i,j}\right) \tag{5.10}$$

By using the Taylor's series expansion, we can show that

$$\frac{\partial^2 \theta_{i,j}}{\partial x^2} \cong \frac{\left(2\theta_{i,j} - \theta_{i+1,j} - \theta_{i-1,j}\right)}{h^2} \tag{5.11}$$

$$\frac{\partial^2 \theta_{i,j}}{\partial z^2} \cong \frac{\left(2\theta_{i,j} - \theta_{i,j+1} - \theta_{i,j-1}\right)}{k^2} \tag{5.12}$$

where h and k are x and z-direction unit distance of the segments as shown in Figure 5.10. By substituting Equations (5.11) and (5.12) into Equation (5.10), we get Equation (5.13).

$$\theta_{i,j}{}^{new} = \frac{h^2 k^2}{2\left(h^2 + k^2\right)} \left(\frac{\theta_{i+1,j} + \theta_{i-1,j}}{h^2} + \frac{\theta_{i,j+1} + \theta_{i,j-1}}{k^2} - f\left(\theta_{i,j}\right) \right) \tag{5.13}$$

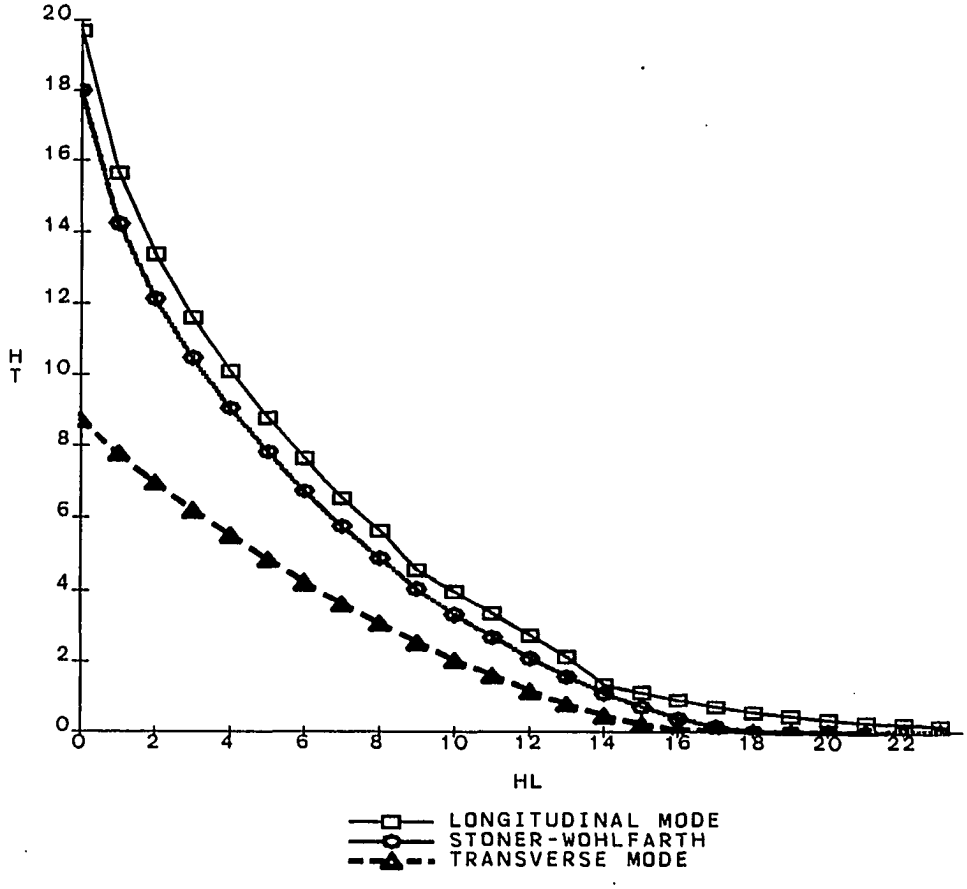

Figure 5.8: Switching threshold

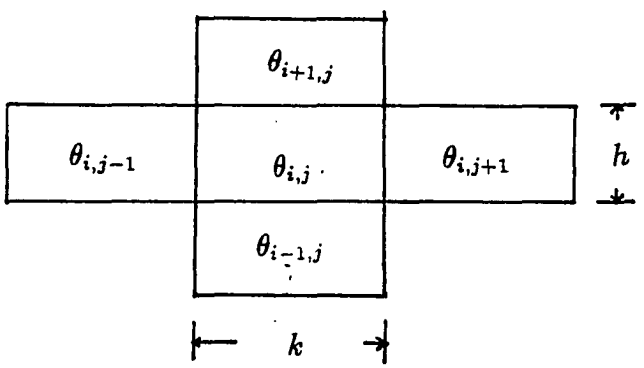

Figure 5.9: Five point method

The new angle $\theta_{i,j}$ is computed from Equation (5.13), which is called the standard five point method [40]. All the other points influence the determination of the new $\theta_{i,j}$ by the demagnetizing field effects.

In updating a value of a point, the adjacent cells play the most important role, the adjacent top and bottom segments especially influence each other by the coupling of demagnetization field. This field is proportional to $1/r^2$, where r is the distance between the magnetic pole and the point of interest. Therefore, faster and more stable convergence can be obtained by updating the top and bottom segments simultaneously.

Because of the geometrical symmetry of the elements when the value at one point is determined, the effect of three other points can be determined without additional calculation from the following relationship between segments.

$$\theta^{top}_{i,j} = \theta^{top}_{Nx-i,Nz-j},$$

$$\theta^{bot}_{i,j} = \theta^{bot}_{Nx-i,Nz-j} \; for \; all \; types \tag{5.14}$$

and

$$\theta^{top}_{i,j} = \pi - \theta^{bot}_{Nx-i,j} = \pi - \theta^{bot}_{i,Nz-j} \; for \; transverse \; mode \tag{5.15}$$

$$\theta^{top}_{i,j} = -\theta^{bot}_{Nx-i,j} = -\theta^{bot}_{i,Nz-j} \; for \; longitudinal \; mode \tag{5.16}$$

where θ^{top} and θ^{bot} designates the angle of top and bottom segments, respectively, and Nx is the number of segments in row i, and Nz the number of segments in column j. The total program is implemented based on the above facts, and its logic can be described as follows:

```
while not converged do begin{while}
    for i = 1, Nx do begin{1-run}
        while not converged do begin{line}
            for i = 1, Nz do begin
                (do point iteration)
            end
        end{line}
    end{1-run}
end{while}
```

In the subsections which follow, the details of point iteration and line iteration will be discussed.

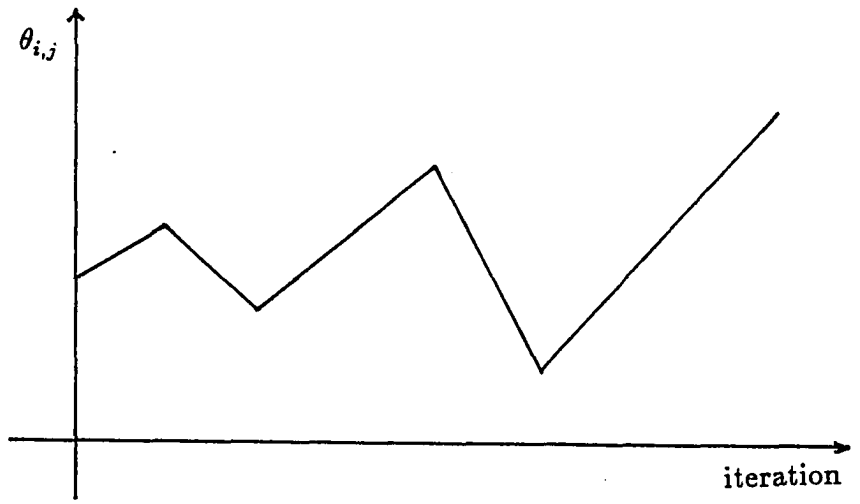

Figure 5.10: Oscillatory behavior of point iteration

5.2.1. Point iteration

When Equation (5.13) is used to change $\theta_{i,j}$, the four magnetic poles adjacent to $\theta_{i,j}$ are also changed. The iteration on $\theta_{i,j}$ is repeated with the updated demagnetizing fields resulting from the new magnetic poles. Since the distance between poles and the point of interest is very short, unstable oscillatory behavior is observed as the iteration on $\theta_{i,j}$ continues. This oscillatory behavior is shown in Figure 5.11. To obtain the convergence two different techniques are used. The first technique is under-relaxation, which can be expressed as Equation (5.17).

$$\theta_{i,j}^{top} = \theta_{i,j}^{old} + \beta\left(\theta_{i,j}^{cal} - \theta_{i,j}^{old}\right) \qquad with \;\; 0 \leq \beta < 1 \tag{5.17}$$

where $\theta_{i,j}^{cal}$ represents the value calculated by Equation (5.13). This technique sacrifices the speed of convergence to get more stable behavior which leads to the

convergence of the point iteration. For $1 \leq \beta < 2$ Equation(5.17) is called the over-relaxation which is commonly used to accelerate convergence.

The second technique is the selective squeezing. Since the divergence comes only from oscillatory behavior, the convergence can be obtained by damping out the oscillatory behavior. Therefore, whenever the oscillatory behavior is observed the newly calculated value is modified by the Equation (5.18).

$$\theta_{i,j}^{new} = \frac{\theta_{i,j}^{old} + \theta_{i,j}^{cal}}{2} \tag{5.18}$$

The selective squeezing method is more difficult to implement since it requires the memory of past behavior. However, it was found that this method is more effective in getting the fast convergence compared to the under-relaxation technique.

5.2.2. Line Iteration

After the point iteration on $\theta_{i,j}^{top}$ and $\theta_{i,j}^{bot}$ is completed with sufficient accuracy, these new values replace the old ones immediately for the calculating of next points. The updating scheme described above is called the Gauss-Seidal method or successive replacement method. Another updating scheme is Jacobi method or simultaneous replacement method in which all the values are updated simultaneously after the final value of the block is obtained. The Gauss-Seidal method is known to converge twice as fast as the Jacobi method [41].

After the calculation on $\theta_{i,j}$ is completed, the next computation is performed on $\theta_{i,j+1}$. This procedure is continued until all the points in the row i are computed. Then, the computations on the points in the row i are repeated until the values in the row i have the sufficient convergence. This procedure is called line iteration.

The reason why the row is selected instead of the column for line iteration is as follows. The rate of convergence for the line iteration scheme is given by Equation (5.19)

$$R = Ad^2 + O\left(d^4\right) \tag{5.19}$$

where A is constant and d is the distance between segments. For our cases, d is $k\left(= 2000\mathring{A}\right)$ for the row iteration and $h\left(= 500\mathring{A}\right)$ for the column iteration.

To implement the Gauss-Seidal method for line iteration the demagnetizing field should be calculated separately for each point while it can be done simultaneously for all points in Jacobi method. Thus, the implementation of Gauss-Seidal method for line iteration requires a little more over heads than the implementation of Jacobi method. After the line iteration on row i is completed, the same line iteration is moved on to the row $i + 1$. This procedure is continued until the whole segments in the elements are covered.

Total of 40 - 80 iterations on the whole elements are performed to get the sufficiently accurate result.

5.3. Results and Discussion

The values of the resulting angles and demagnetizing fields of the various modes of elements are depicted as the amplitudes in Figure 5.11-5.22. Because of the symmetry of the elements only the left half of the elements are pictured. We can see that the 2-dimensional results are very similar to those of 1-dimensional results as shown in Figure 5.3-5.4 at the middle of the element.

The angle distribution of the various modes of elements are very smooth and reasonable for all elements except for the longitudinal square type element. In the case of the longitudinal square type element we can see that two Néel walls are formed parallel to the long dimension of the element for a moderate external field condition. This behavior seems to be due to the fact that the boundary values which lie in the hard direction at the edge of the element are exaggerated. The x-directional demagnetizing field of this type of element is depicted in Figure 5.21 to show the wall formation.

Generally, we can expect that the angles at the edges are tipped slightly to make a small angle with the boundary. The perturbed angle at the boundary tends to be maximum at the edges which run parallel to the short dimension of the element. Especially, when the boundary condition does not favor the anisotropy at the edges, the contradiction reaches the maximum which leads to the biggest angle perturbation at the edges. Therefore, the transverse diamond type elements generate the smoothest angle distribution of all types of elements. More study in boundary conditions is expected to lead to more reasonable solutions and remains as future work.

The results of two 2-dimensional solution at the middle of the elements are compared with the 1-dimensional results in Figure 5.23 and 5.24 for longitudinal mode and transverse mode, respectively. As shown in the figures the two results are very close to each other, which supports the validity of both methods.

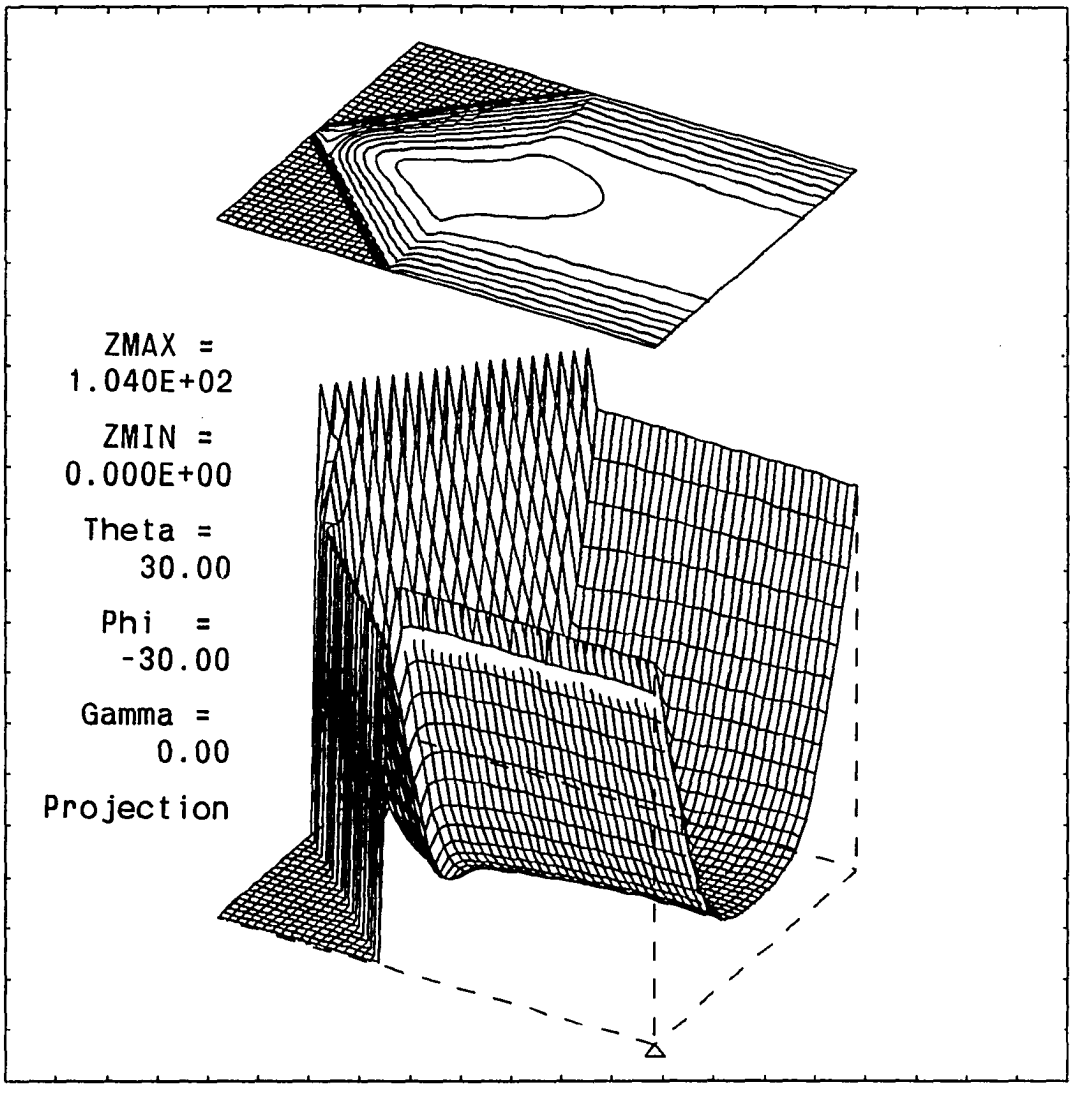

Figure 5.11: Angle(in degree) of transverse diamond elements with $H_x = -1.0$ and $H_z = 5.6\ Oe$

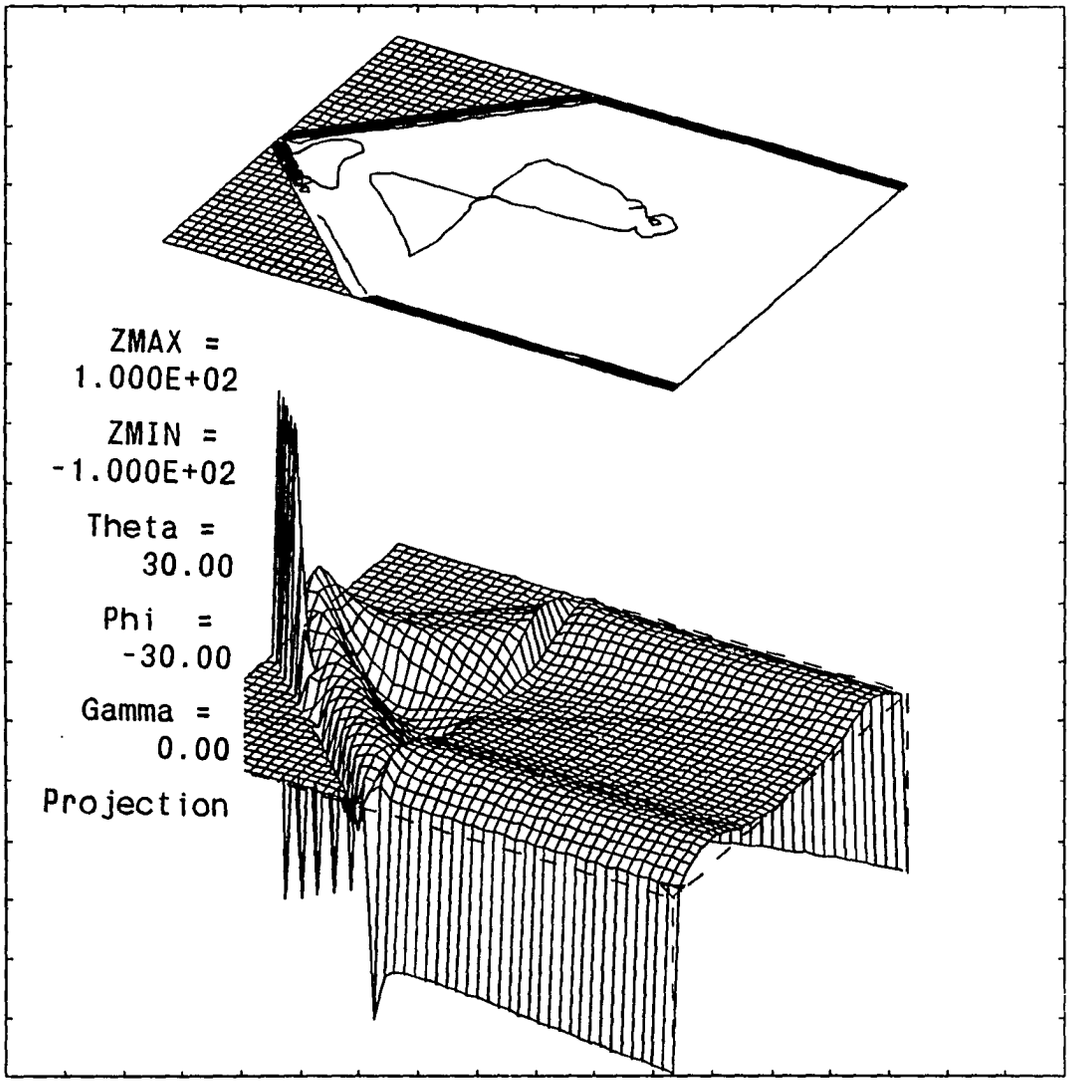

Figure 5.12: H_{dx} of transverse diamond elements with $H_x = -1.0$ and $H_z = 5.6\ Oe$

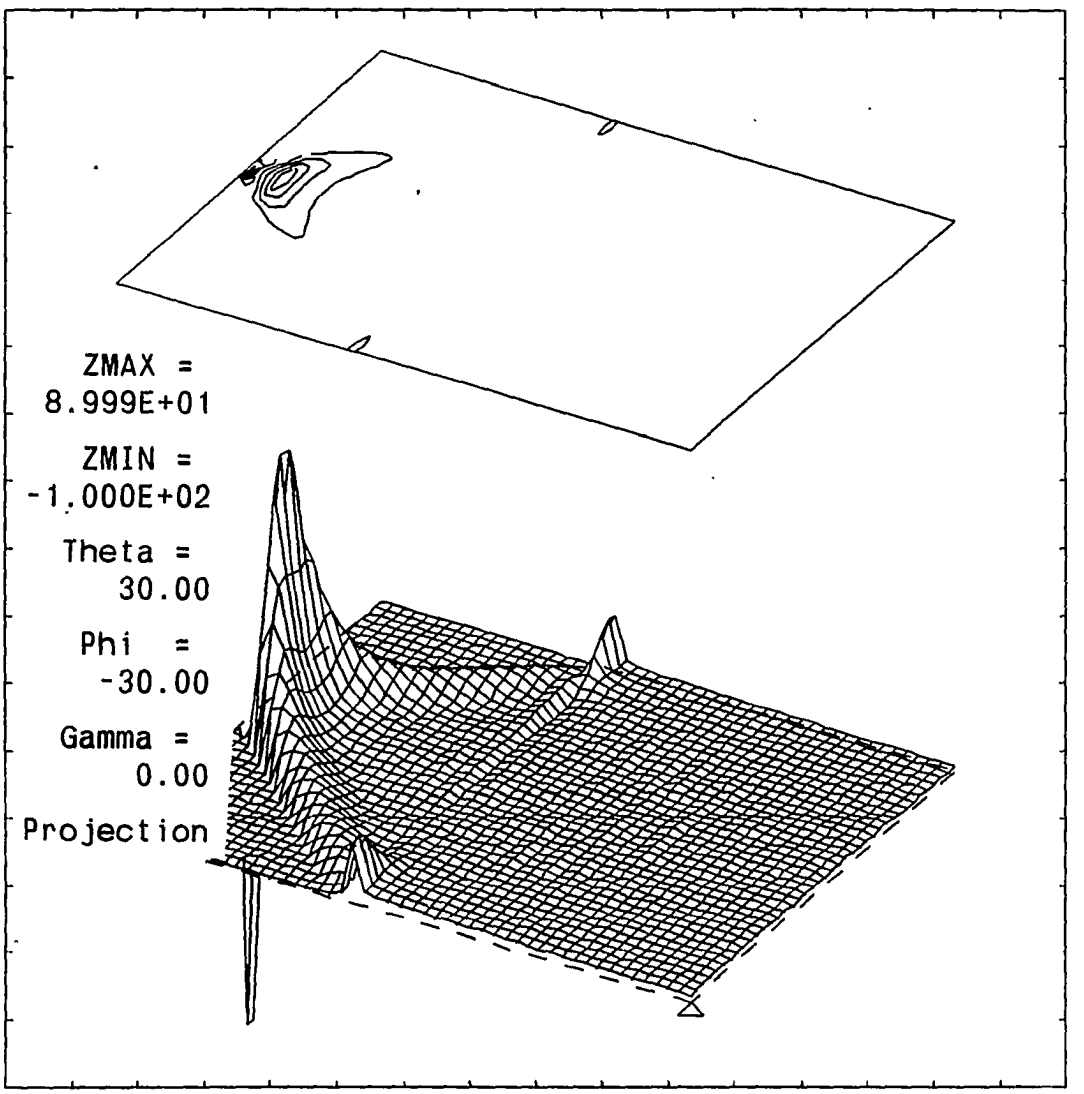

Figure 5.13: H_{dz} of transverse diamond elements with $H_x = -1.0$ and $H_z = 5.6\ Oe$

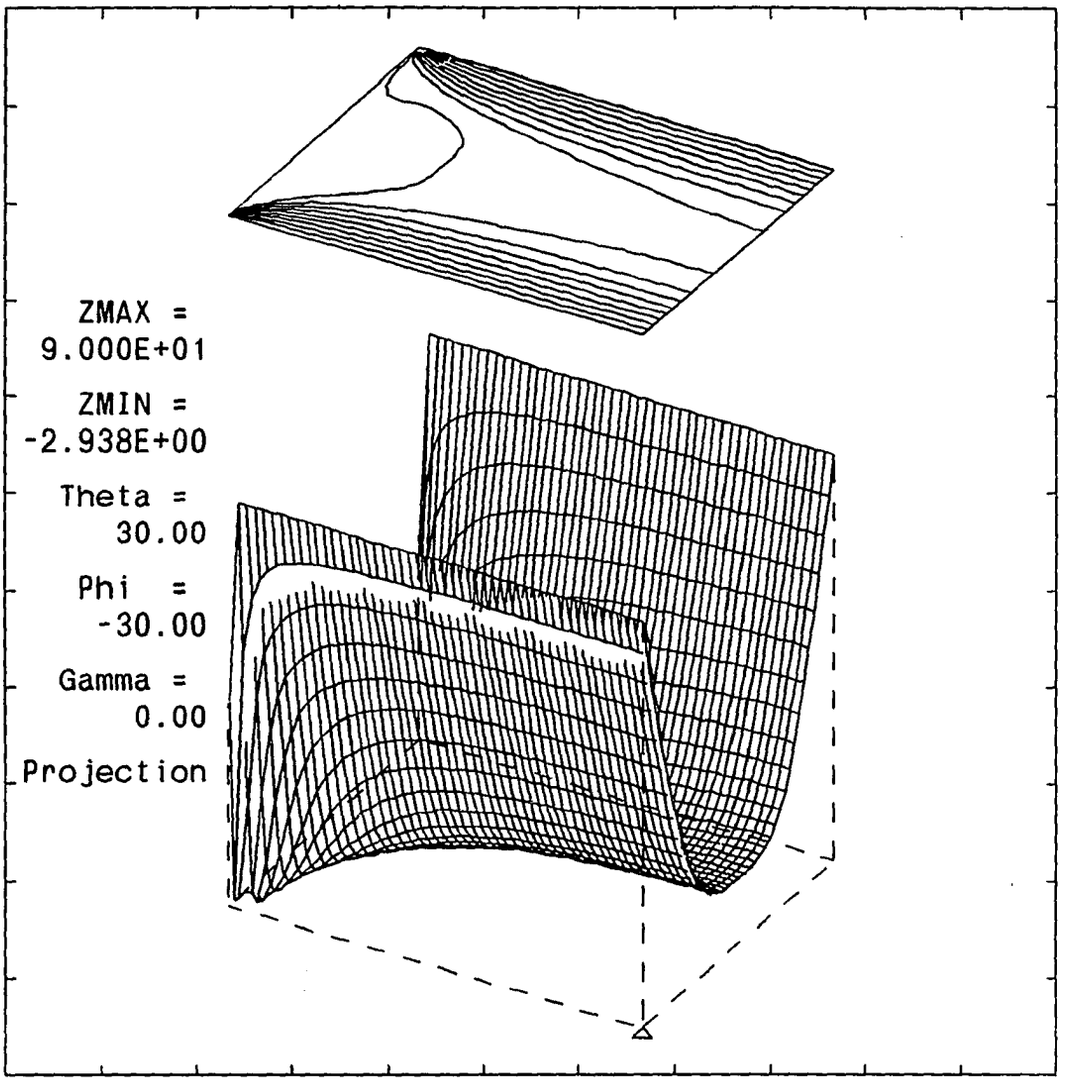

Figure 5.14: Angle(in degree) of transverse square elements with $H_x = -1.0$ and $H_z = 5.6\ Oe$

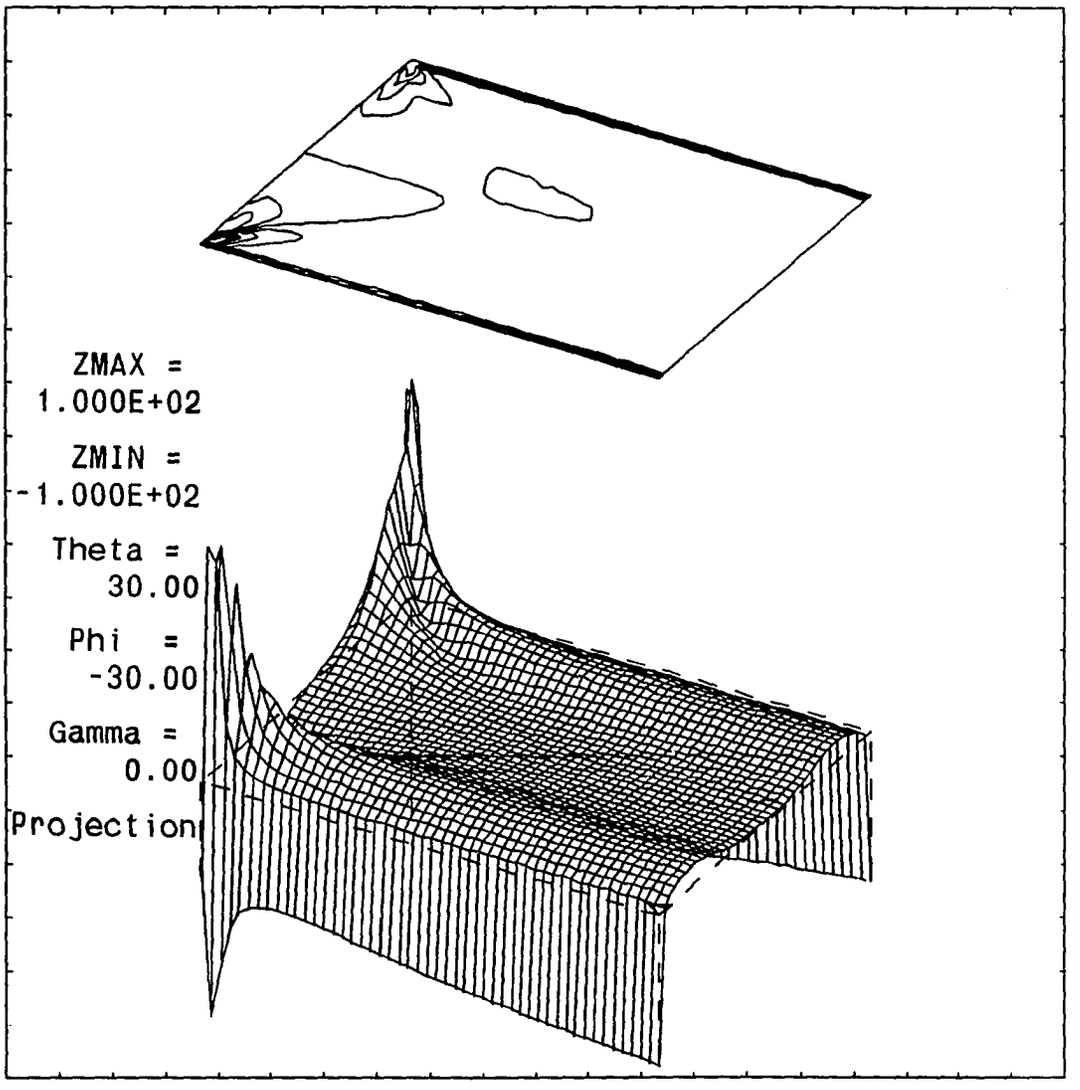

Figure 5.15: H_{dx} of transverse square elements with $H_x = -1.0$ and $H_z = 5.6\ Oe$

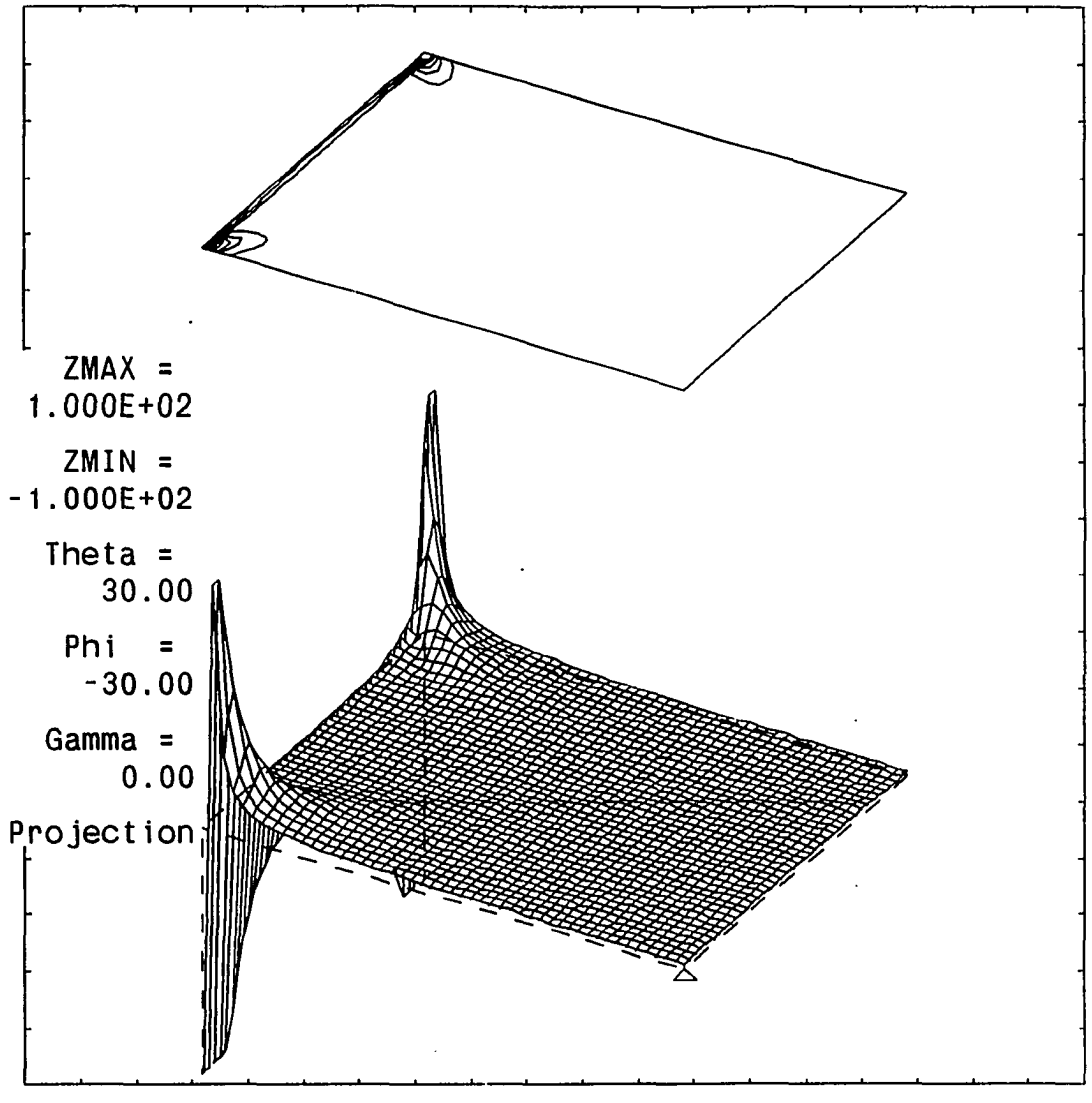

Figure 5.16: H_{dz} of transverse square elements with $H_x = -1.0$ and $H_z = 5.6\ Oe$

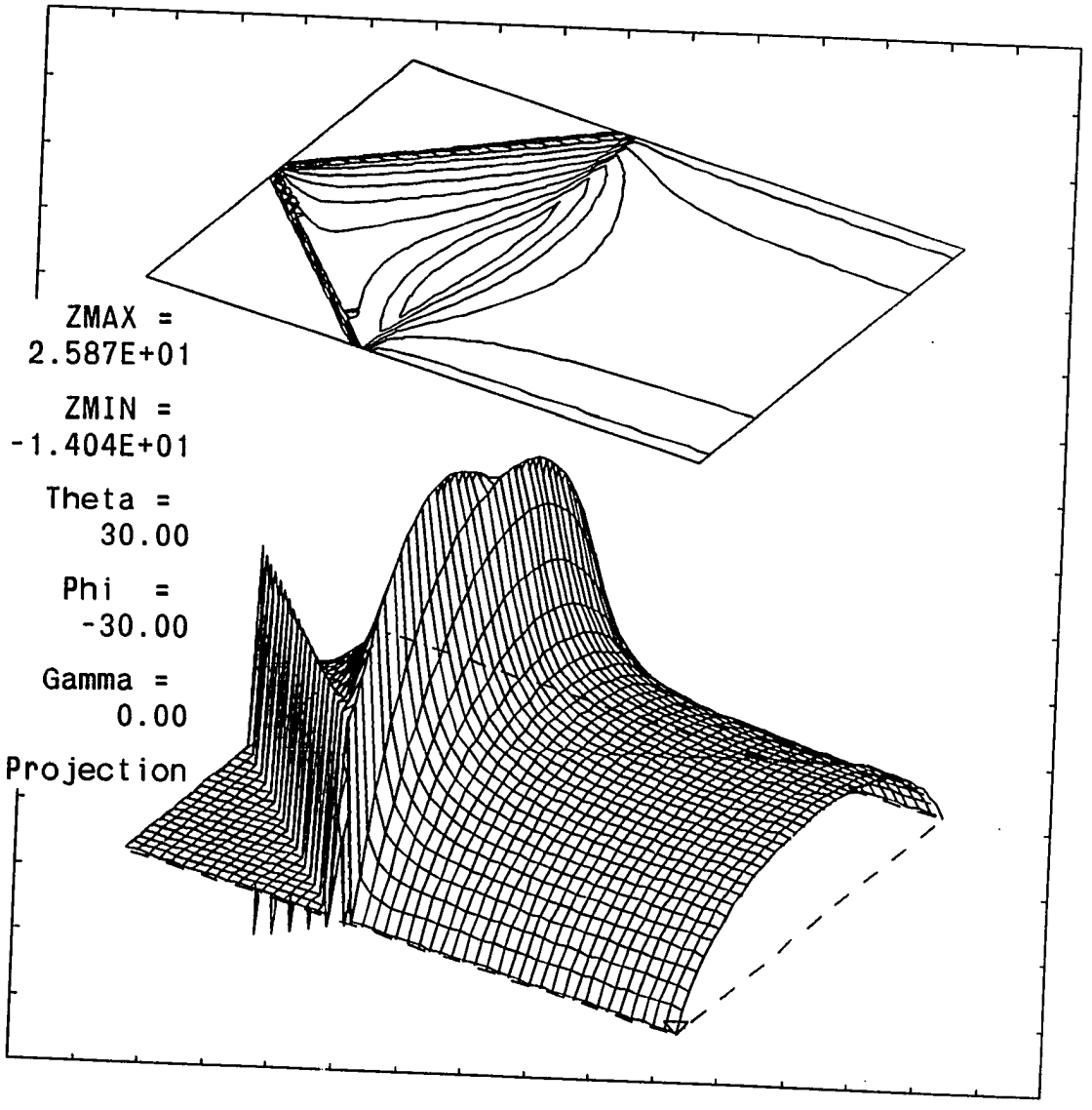

Figure 5.17: Angle(in degree) of longitudinal diamond elements with $H_x = 2.0$ and $H_z = -1.0\ Oe$

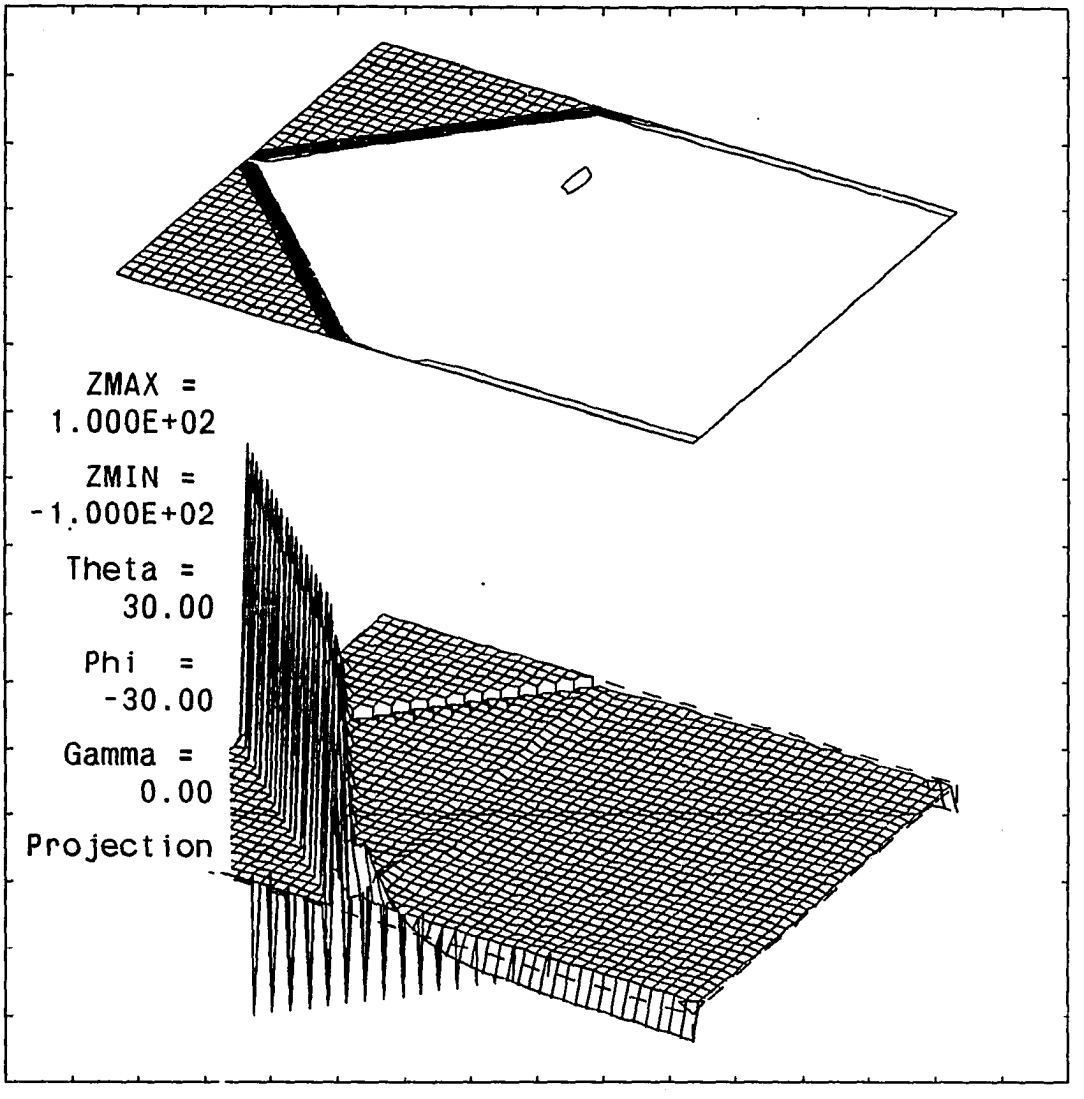

Figure 5.18: H_{dx} of longitudinal diamond elements with $H_x = 2.0$ and $H_z = -1.0$ Oe

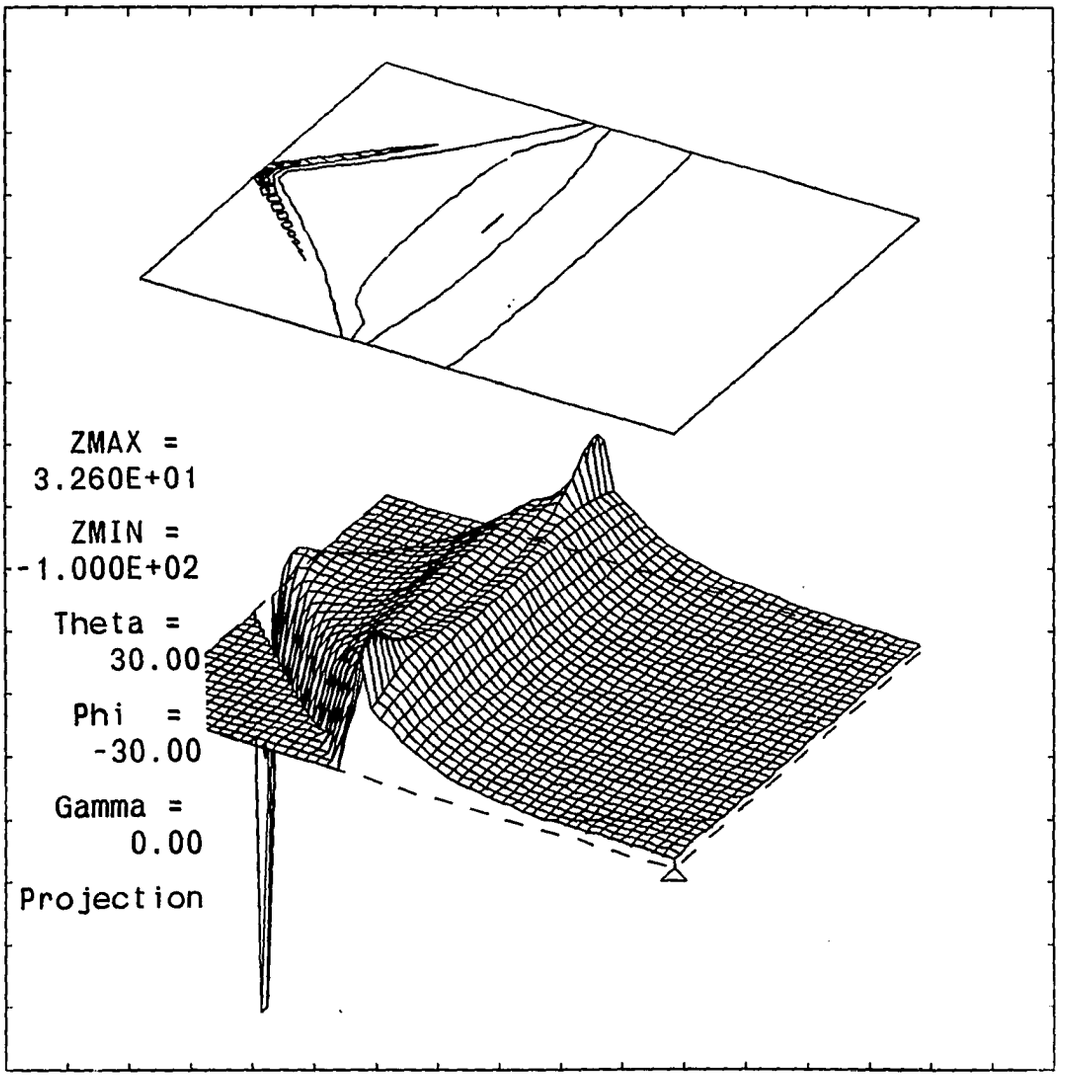

Figure 5.19: H_{dz} of longitudinal diamond elements with $H_x = 2.0$ and $H_z = -1.0$ Oe

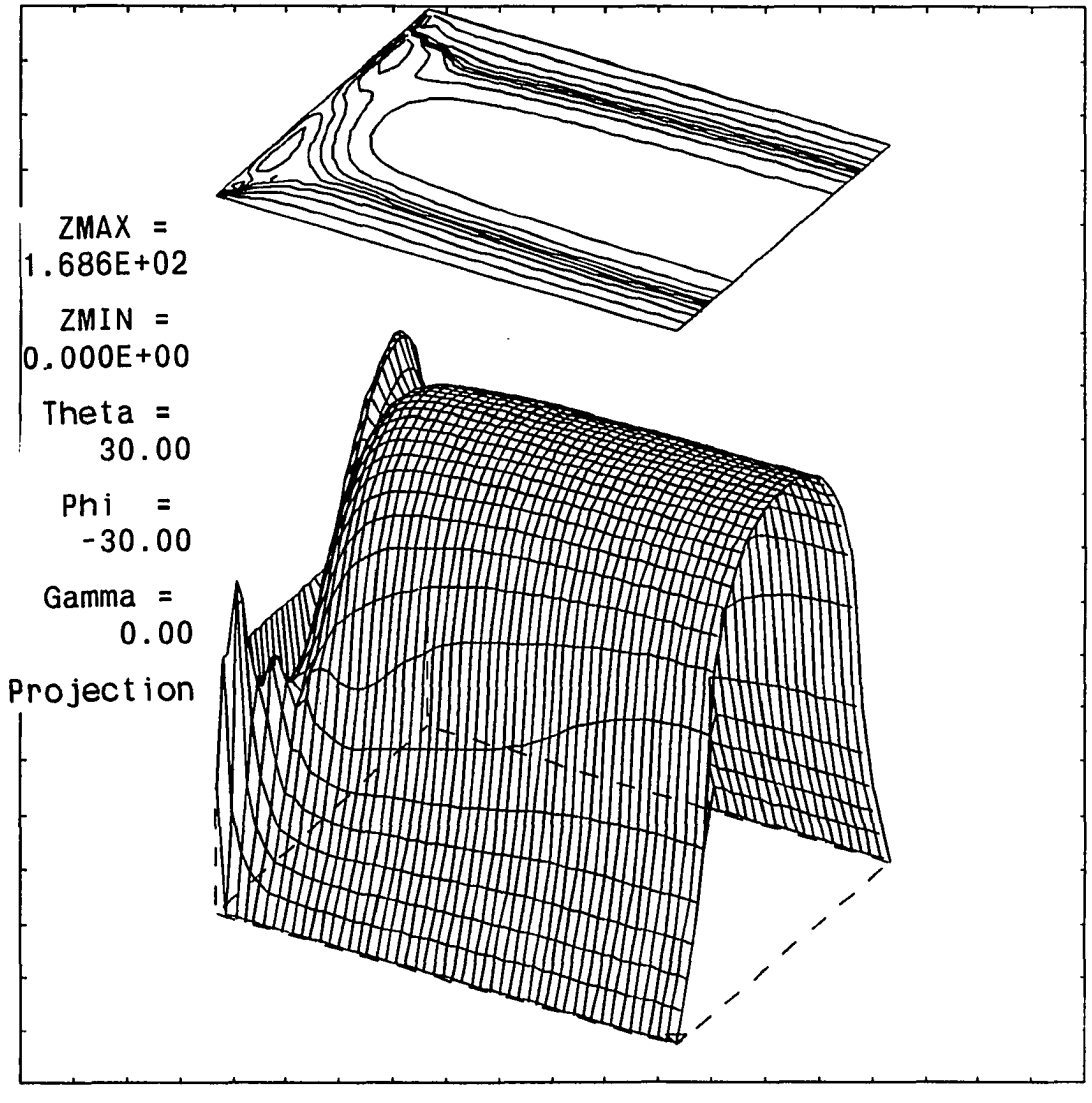

Figure 5.20: Angle(in degree) of longitudinal square elements with $H_x = 2.0$ and $H_z = -1.0\ Oe$

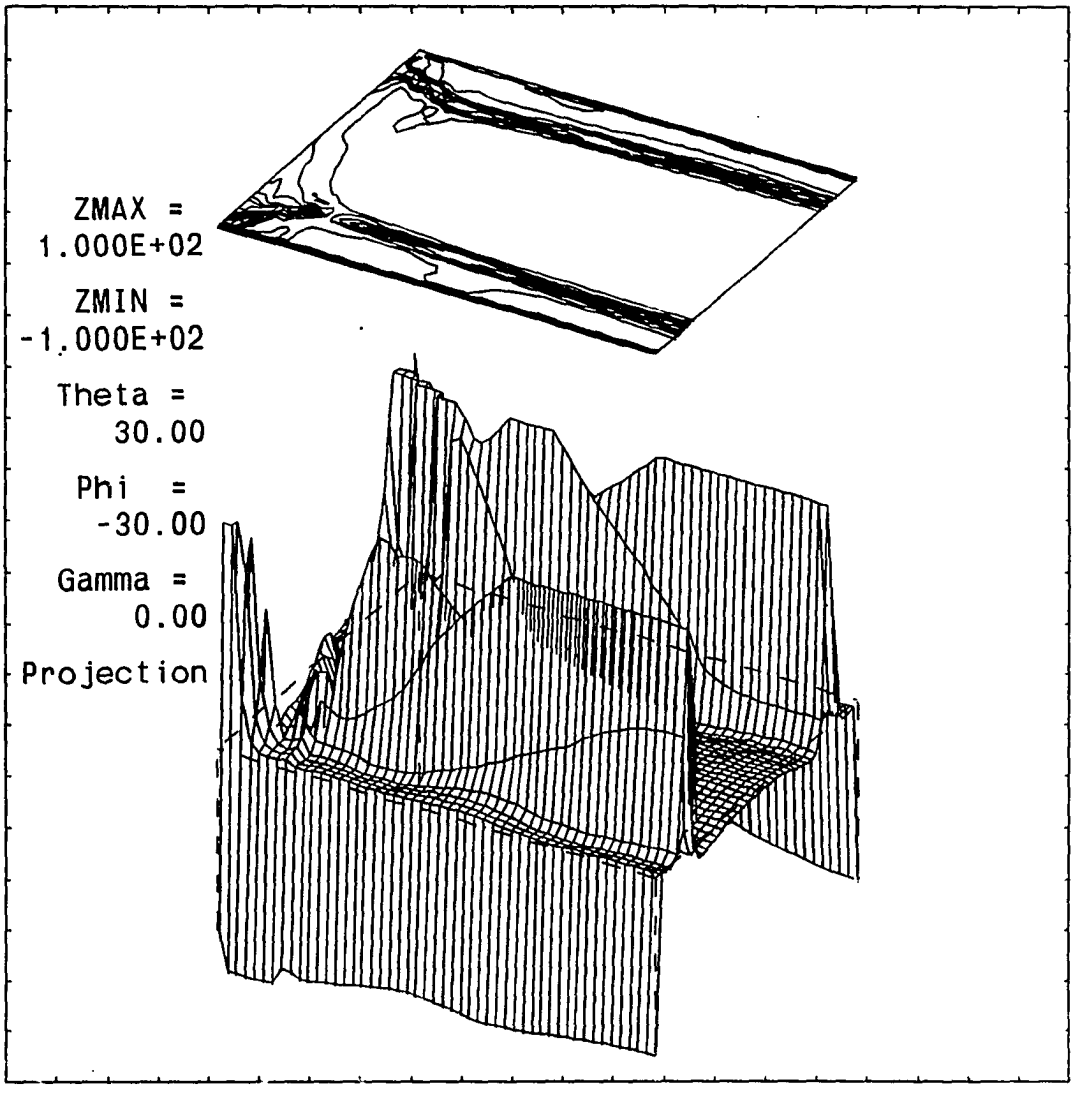

Figure 5.21: H_{dx} of longitudinal square elements with $H_x = 2.0$ and $H_z = -1.0$ Oe

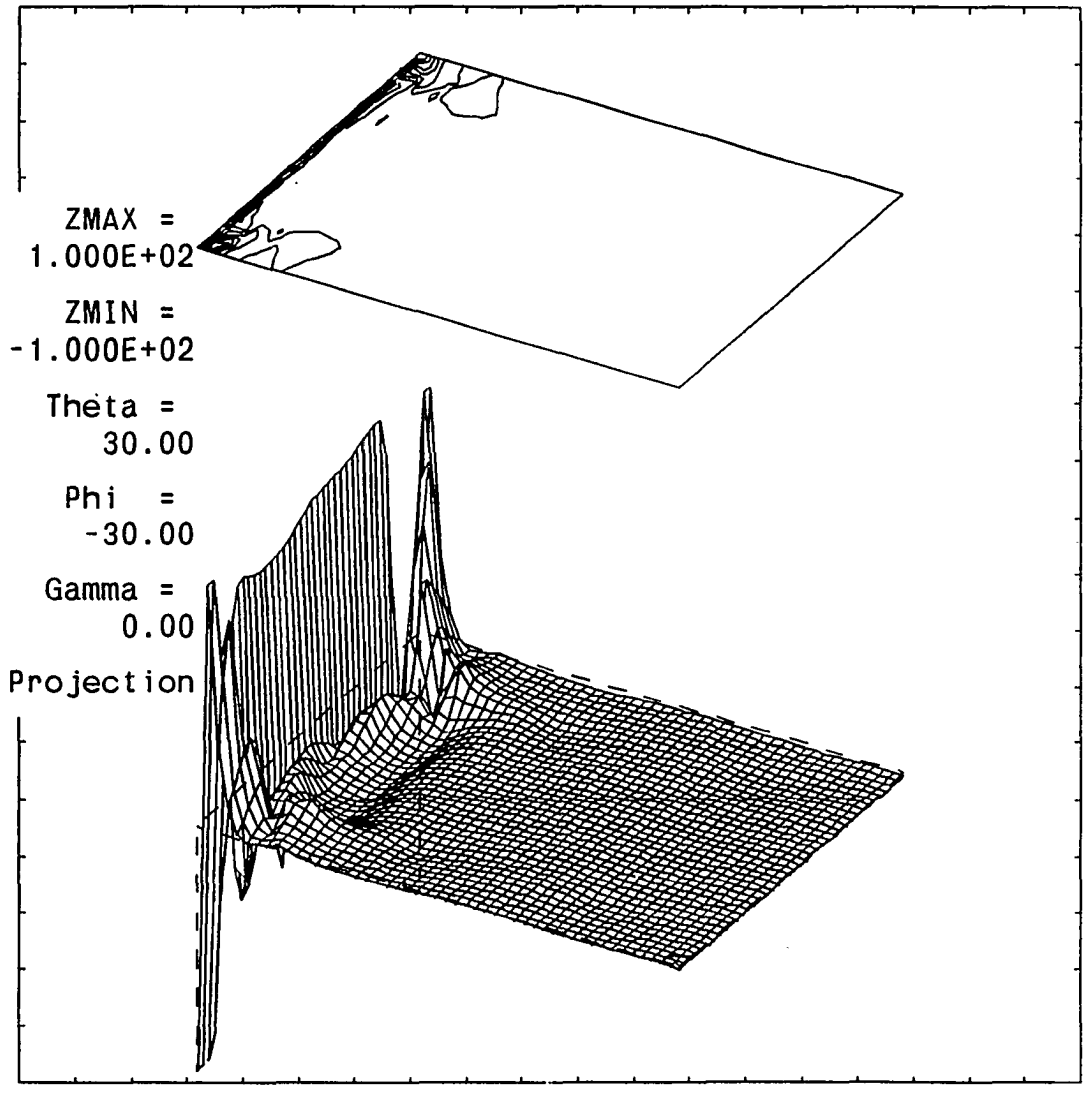

Figure 5.22: H_{dz} of longitudinal square elements with $H_x = 2.0$ and $H_z = -1.0\ Oe$

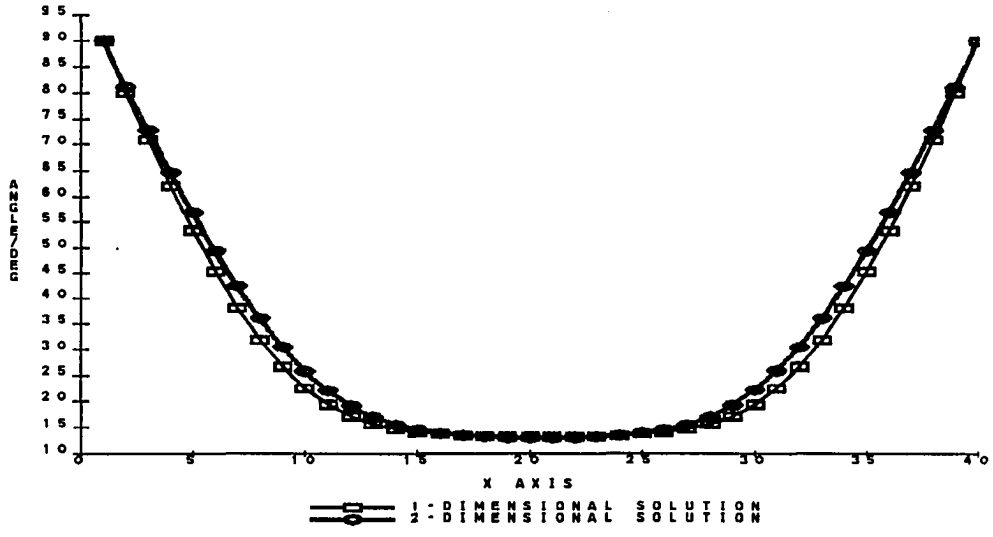

Figure 5.23: Comparison between 1-dimensional and 2-dimensional solutions of longitudinal mode elements

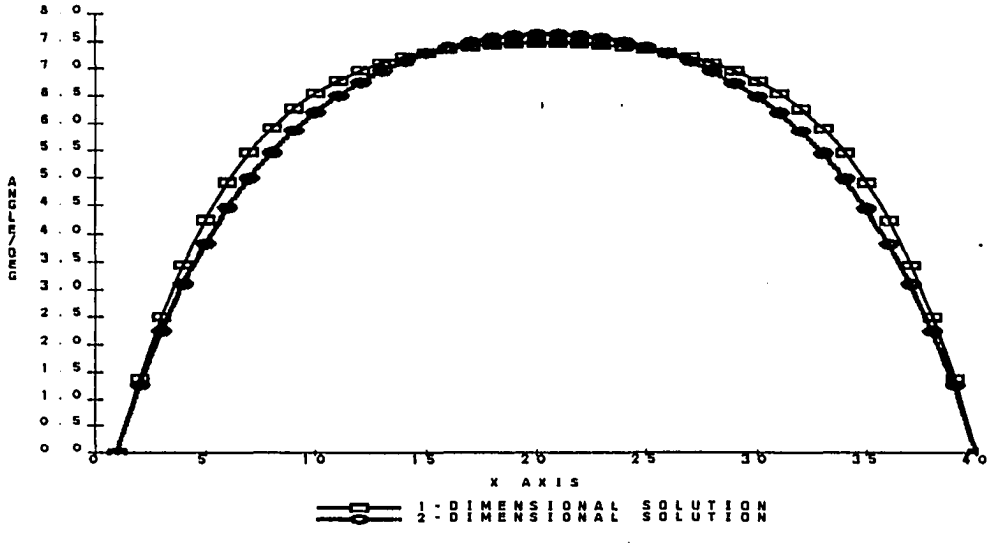

Figure 5.24: Comparison between analytic and numeric solutions of transverse elements

6. CONCLUSIONS AND FUTURE WORK

It is shown that the 2-dimensional micromagnetic equation can be used as a very effective analysis tool for sandwich-structured thin film elements. In solving the micromagnetic equation point iteration plays a critical role since it suppresses the divergent behavior caused by the demagnetizing field effect. For the types of elements considered, the transverse diamond type elements shows the smoothest angle distribution.

The followings remain as future work:

1. As mentioned before, our assumption on boundary conditions meet some controversy at the short edge of the element. A new solution using the original boundary condition given in Equation (2.5) is expected to give better results.

2. The external fields generated by the word line and sense current are assumed to be constant in this treatment. A more reasonable assumption on the external field condition will give the better results at the edge.

3. For the rigorous treatment addition of a y-direction variation of angle is recommended.

4. Finally, more work on acceleration techniques for numerical solution will be helpful. Bloomberg [42] found that more stable behavior can be obtained

by replacing field $\vec{H}$ with the flux $\vec{B}$ in the micromagnetic equation. Such stable behavior means that the we can use acceleration technique such as over-relaxation instead of selective squeezing or under-relaxation technique.

7. ACKNOWLEDGEMENT

First of all, I would like to thank my major professor, Dr. Smay for his encouragement and concern all through my graduate work. The same amount of thanks are directed to my project director, Dr. Pohm whose insight and encouragement was critical to this work. I also thank Dr. Comstock who made our project a pleasant place to work in. Thanks are extended to my committee Dr. Oldehoeft and Dr. Grosvenor. Special thanks are for Honeywell Inc. and CDC for their financial support.

I would also like to thank my wife, Yaesun and my son, Seungwoo who always gave me refreshment and joy of life. Finally, I would like to thank my parents who always watch over me from Heaven. I always feel that I am with them and if this work gives them something to be proud of their son, it will be my utmost happiness.

8. BIBLIOGRAPHY

[1] T. R. Mcguire and R. I. Potter. "Anisotropic magnetoresistance in ferromagnetic 3d alloys." *IEEE Trans. on Magnetics* MAG-11 (1975):1018.

[2] D. A. Thomson, L. T. Romankiw and A. F. Mayadas. "Thin film magnetoresistor in memory, storage, and related applications." *IEEE Trans. on Magnetics* MAG-11 (1975):1039.

[3] R. P. Hunt. "A magnetoresistive reaout transducer." *IEEE Trans. on Magnetics* MAG-7 (1971):150.

[4] D. A. Thompson. "Magnetoresistive transducers in high-density magnetic recording." *Proc. AIP Conf.* 20 (1974):528.

[5] G. V. Kelly and R. A. Ketcham. "An analysis of the effect of shield length on the performance of magnetoresistive heads." *IEEE Trans. on Magnetics* MAG-14 (1978):515.

[6] T. N. Casselman and S. A. Hanka. "Calculation of the performance of a magnetoresistive permalloy magnetic field sensor." *IEEE Trans. on Magnetics* MAG-16 (1981):461.

[7] S. K. Decker and C. Tsang. "Magnetoresistive response of small permalloy features." *IEEE Trans. on Magnetics* MAG-16 (1980):643.

[8] W. F. Druyvesteyn, J. A. C. van Ooyen, L, Postma, E. L. M. Raemaekers, J. J. M. Ruigrok, J. de Wilde. "Magnetoresistive heads." *IEEE Trans. on Magnetics* MAG-17 (1981):2884.

[9] C. Tsang and S. K. Decker. "Study of domain formation in small permalloy magnetoresistive elements." *J. Appl. Phys.* 53 (1982):2602.

[10] C. Tsang. "Magnetics of small magnetoresistive sensors." *J. Appl. Phys.* 55 (1984):2226.

[11] M. H. Kryder, K. Y. Ahn, N, J. Mazzeo, S. Schwarzl, and S. M. Kane. "Magnetic properties and domain structures in Narrow NiFe Stripes." *IEEE Trans. on Magnetics* MAG-16 (1980):99.

[12] J. A. C. van Ooyen, W. F. Druyvesteyn and L. Postma. "Magnetoresistance in laminated NiFe films." *J. Appl. Phys.* 53 (1982):2596.

[13] J. L. Berchier, K. Solt and T. Zajc. "Magnetoresistive switching of small permalloy sandwich structures." *J. Appl. Phys.* 55 (1984):487.

[14] C. Tsang and R. E. Fontana. "Fabrication and wafer testing of barber-pole and exchange-biased narrow-track MR sensors." *IEEE Trans. on Magnetics* MAG-18 (1982):1149.

[15] L. J. Schwee, H. R. Irons, and W. E. Anderson. "The crosstie memory." *IEEE Trans. on Magnetics* MAG-12 (1976):608.

[16] S. Middlehoek. "Ferromagnetic domains in thin NiFe films." *Ph.D Thesis,* Univ. Amsterdam, 1961.

[17] L. J. Schwee, P. E. Hunter, K. A. Restorff, and M. T. Schephard. "The concept and initial studies of a crosstie random access memory (CRAM)." *J. Appl. Phys.* 53 (1983).

[18] D. S. Lo, V. M. Benrud, G. J. Cosimini, L. H. Johnson, G. G. Nelson, M. C. Paul, and E. J. Torok. "Cross-tie shift register." *J. Appl. Phys.* 50 (1979):2295.

[19] A. V. Pohm and C. S. Comstock. "0.75, 1.25 and 2 μm wide MR transducers." *J. Magnetism and Magnetic Materials* 54-57 (1986):1667.

[20] N. Smith. "Micromagnetic analysis of a coupled thin-film self-biased magnetoresistive sensor." *IEEE Trans. on Magnetics* MAG-23 (1987):259.

[21] E. D. Torre. "Numerical micromagnetic calculations." *IEEE Trans. on Magnetics* MAG-21 (1979):1225.

[22] J. F. Dillon, Jr. "Domains and domain walls." *Chapter 9 of Magnetism edited by G. T. Rado and H. Suhl.* New York:Academic Press, 1963.

[23] W. F. Brown, Jr. "Micromagnetics." New York:John Wiley & Sons, 1963

[24] L. Landau and E. Lifshitz. *Physik. Z. Sowjetunion* 8 (1935):153.

[25] S. Chikazumi and S. H. Charap. "Physics of magnetism." New York:Krieger Publishing Company, 1986

[26] H. A. M. van den Berg. "Micromagnetics and domains in soft ferromagnetic media." *Ph.D Thesis,* Deft University Press, 1984.

[27] S. Shtrikman and D. Treves. "Micromagnetics." *Chapter 8 of Magnetism, edited by G. T. Rado and H. Suhl.* New York:Academic Press, 1963.

[28] W. F. Brown, Jr. and A. E. Labonte. "Structure and Energy of one-dimensional walls in ferromagnetic thin films." *J. Appl. Physics* 36 (1965):1380.

[29] A. E. Labonte. "Two-dimensional Bloch-type domain walls in Ferromagnetic films." *J. Appl. Physics* 40 (1969):2450.

[30] E. D. Torre. "Magnetization calculation of fine particles." *IEEE Trans. on Magnetics* Mag-20 (1986):484.

[31] D. R. Fredkin, and T. R. Koehler. "Numerical micromagnetics by the finite element." *IEEE trans. on Magnetics* MAG-23 (1987):3385.

[32] A. V. Pohm, C. S. Comstock and L. A. Pearey. "Submicron MR memory elements : Report #1." Iowa State University, Project 1677, 1983.

[33] B. D. Cullity. "Introduction to magnetic materials." Reading MA:Addison-Wesley, 1972.

[34] A. V. Pohm, C. S. Comstock and L. A. Pearey "Submicron MR memory elements : Report #2." Iowa State University, Project 1677, 1984.

[35] A. V. Pohm, T. M. Daughton, C. S. Comstock, H. Y. Yoo and J. H. Hur. "Threshold properties of 1,2 and 4μm multilayer MR memory cells." *IEEE Trans. on Magnetics* MAG-23 (1987):2575.

[36] A. V. Pohm, C. S. Comstock, L. A. Pearey, J. Lutz, S. Irwin and R. Lee. "Submicron MR memory elements : Report #3." Iowa State University, Project 1677, 1985.

[37] W. F. Brown Jr. "Magnetostatic principal in ferromagnetism." Hague, Netherlands:North-Holland Publishing Co., 1962.

[38] M. E. Schabes and A. Aharoni. "Magnetostatic interaction fields for a three-dimensional array of ferromagnetic cubes." *IEEE Trans. on Magnetics* MAG-23 (1987):3882.

[39] C. S. Comstock, H. Y. Yoo and A. V. Pohm. "Perturbation to Stoner-Wohlfarth threshold in 2 x 20 μm MR memory elements." *J. Appl. Physics* (April 1988).

[40] G. D. Smith. "Numerical solution of partial differential equation." Oxford:Oxford University Press, 1978.

[41] E. Isaacson and H. B. Keller. "Analysis of numerical method." New York:John Wiley and Sons, 1966.

[42] D. S. Bloomberg. "Implementation of MB algorithm for nonlinear magnetostatics." *IEEE Trans. on Magnetics* MAG-23 (1987):3927.